EUROPEAN COMMISSION

Community Research

SEVENTH FRAMEWORK PROGRAMME

ARCHER

Collaborative Project (CP)

Co-funded by the European Commission under the Euratom Research and Training Programme on Nuclear Energy within the Seventh Framework Programme

Grant Agreement Number : 269892

Start date : 01/02/2011 Duration : 48 Months

www.archer-project.eu

Neutronic modelling of the HFR-EU1 and HFR-EU1bis experiments

Authors : HAECK Wim (IRSN)

ARCHER - Contract Number: 269892
Advanced High-Temperature Reactors for Cogeneration of Heat and Electricity R&D
EC Scientific Officer: Dr. Panagiotis Manolatos

Document title	Neutronic modelling of the HFR-EU1 and HFR-EU1bis experiments
Author(s)	HAECK Wim
Number of pages	43
Document type	Deliverable
Work Package	WP 32
Document number	D32.31
Issued by	NRG
Date of completion	19/06/2014
Dissemination level	Confidential, only for members of the consortium (including the Commission Services).

Summary

Final report for SP3 Task 3.2.3

Approval

Date	By
07/07/2014	Mathias LAURIE
07/07/2014	Mathias LAURIE
07/07/2014	Steven KNOL

Distribution list

Name	Organisation	Comments
P. Manolatos	EC DG RTD	Through the EC participant portal
All beneficiaries	ARCHER	Through the private online workspace

RAPPORT

IRSN
INSTITUT
DE RADIOPROTECTION
ET DE SÛRETÉ NUCLÉAIRE

Faire avancer la sûreté nucléaire

HFR-EU1 depletion calculations

ARCHER Project Deliverable D32.31

W. HAECK

Rapport n° PSN-EXP/SNC/2014-135

Pôle sûreté des installations et des systèmes nucléaires
Service de Neutronique et des risques de Criticité

IRSN
INSTITUT
DE RADIOPROTECTION
ET DE SÛRETÉ NUCLÉAIRE

Pôle sûreté des installations et des systèmes nucléaires
Service de Neutronique et des risques de Criticité
Bâtiment 25
B.P. 17,
92262 Fontenay-aux-Roses Cedex

HFR-EU1 depletion calculations

ARCHER Project Deliverable D32.31

Rapport n° PSN-EXP/SNC/2014-135

	Rédacteur(s) *Author(s)*	Vérificateur(s) *Reviewer(s)*	Chef d'unité *Head of unit*	Chef de service *Head of department*	Directeur *Director*
Nom *Name*	W. HAECK		S. PIGNET	E. LÉTANG	J.-C. MICAELLI
Date	10/4/2014		12/4/2014	10/6/2014	
Visa	W Haeck		S Pignet		

Qualité *Quality*	
Nom *Name*	J.-M. GOMIT
Date	10/06/2014
Visa	

Projet *Project*	
Nom *Name*	
Date	
Visa	

PSN/recherche/FRM-006 03-13

IRSN
INSTITUT
DE RADIOPROTECTION
ET DE SÛRETÉ NUCLÉAIRE

Fiche descriptive du rapport
Report description sheet

Titre

HFR-EU1 depletion calculations

Sous-titre

ARCHER Project Deliverable D32.31

Title

HFR-EU1 depletion calculations

Sub-Title

ARCHER Project Deliverable D32.31

Auteur/author(s) : **W. HAECK**

Type de document : *Document type:*	**Rapport Technique**	Date de diffusion : *Distribution date:*	**Juin 2014**
Référence(s) :	**PSN-EXP/SNC/2014-135**	E-mail de l'auteur :	**wim.haeck@irsn.fr**
Elément DPPA	**AF14.23**		

Mots-clés (Max. 5) :	ARCHER, VESTA, HTR
Key-words (Max. 5):	ARCHER, VESTA, HTR

RÉSUMÉ

ABSTRACT

This report presents the final conclusions for the SP3 Task 3.2.3 (HFR-EU1 Irradiation modelling) of the ARCHER project. The objective of this task was to provide a source term of the TRISO particles in the fuel pebbles and accurate neutronics data for fuel performance calculations such as single group averaged cross sections as a function of time. To fullfill this objective, a new model that takes into account the variation as a function of burn up of the isomeric branching ratio for isomeric states (such as ^{242m}Am or ^{110m}Ag) has been implemented in the VESTA software. This has been applied to the HFR-EU1 irradiation experiment (in which several fuel pebbles were irradiated in the HFR in Petten).

HISTORIQUE DES MODIFICATIONS/CHANGE HISTORY

Indice de révision *Revision*	Date	Auteur *Author*	Pages ou paragraphes modifiés *Pages or paragraphs changed*	Nature des modifications *Nature of the changes*
A		W. HAECK		Initial document

CONTENTS

1 Introduction **6**

2 A burn up dependent isomeric branching ratio treatment **7**
2.1 Introduction 7
2.2 A general burn up dependent treatment 8
2.3 Implementation in VESTA 11
2.3.1 Nuclear data treatment 11
2.3.2 Using the multi-group binning approach 12
2.3.3 Using Monte Carlo estimators 14
2.3.4 Validation of the implementation 16
2.3.5 Comparison with ORIGEN library values 17

3 Modelling HFR-EU1 **19**
3.1 The HFR-EU1 experiment 19
3.2 Initial material compositions 19
3.3 Neutron spectra 20
3.4 Irradiation history 22

4 Results for HFR-EU1/3 and HFR-EU1/4 **26**
4.1 Calculation characteristics and reported results 26
4.2 Burn up values 26
4.3 Comparison with activity measurements 27
4.4 Nuclide compositions 31
4.4.1 Actinides 31
4.4.2 Fission products 34
4.5 Power production 39

5 Conclusions **41**

1 INTRODUCTION

The High Temperature Reactor (HTR) is a helium-cooled graphite moderated nuclear reactor concept which combines high safety with high efficiency. This kind of reactor is particularly suitable for operating in cogeneration mode, by supplying of heat and electricity specifically for the European process industry, as an alternative for fossil fuel burning. Europe has a strong history of HTR development and has focused the developments on robust safety, appropriate size and high temperature heat generation. The ARCHER project aims to move this technology base forward by extending knowledge of state-of-the-art European High Temperature Reactors by supporting a nuclear cogeneration demonstration.

The ARCHER project's aims are in line with the Sustainable Nuclear Energy Technology Platform's (SNETP) plans, set out in its Strategic Research Agenda (SRA) and Deployment Strategy (DS). The state-of-the-art of HTR technology has been established mainly by the former European and United States HTR programmes, which were active until the end of the 1980s. ARCHER builds on this, and on the large European HTR technology base established in previous EU Framework Programmes (FP) such as the FP7 projects RAPHAEL and EUROPAIRS ('End User Requirement fOr Process heat Applications with Innovative Reactors for Sustainable energy supply') and the nuclear cogeneration working group in SNETP.

From a general point of view, the R&D activities in ARCHER are split into four key areas:
- evaluating and assessing the system integration of an HTR in connection to industrial processes;
- resolving open questions regarding confirmation of HTR safety, as preparation for a licensing framework;
- providing a basic insight into fuel behaviour to support fuel performance code and support robust demonstrator design;
- progressing HTR and VHTR technology developments on materials and component technology by developing, building and testing an advanced heat exchanger prototype putting Europe at the forefront of advances in this technology.

The present report is issued in the framework of Task 3.2.3 (HFR-EU1 Irradiation modelling) of SP3 on fuel behaviour and corresponds with Deliverable D32.31. The objective is to provide a source term of the TRISO particles in the fuel pebbles and accurate neutronics data for fuel performance calculations such as single group averaged cross sections as a function of time. To fullfill this objective, a new model that takes into account the variation as a function of burn up of the isomeric branching ratio for isomeric states (such as ^{242m}Am or ^{110m}Ag) has been implemented in the VESTA software. This has been applied to the HFR-EU1 irradiation experiment (in which several fuel pebbles were irradiated in the HFR in Petten).

This report is structured as follows. Chapter 2 deals with the development of the new features of the VESTA software to take into account a burn up dependent isomeric branching ratio treatment. This chapter also provides an overview of the methodology used by VESTA to properly calculate the required data needed for performing depletion calculations. Chapter 3 gives an overview of the HFR-EU1 experiment and the way this irradiation was modelled using the VESTA software and chapter 4 presents the results for the HFR-EU1/3 and HFR-EU1/4 pebbles (for which experimental results are available).

2 A BURN UP DEPENDENT ISOMERIC BRANCHING RATIO TREATMENT

2.1 Introduction

The reaction cross section data used during depletion calculations give precise information on the disappearance of a particular nuclide. The daughter nuclide created in the reaction is however another matter. An obvious example is fission in which numerous different fission products can be created. Depletion codes therefore use direct fission yield data to properly account for the creation of these fission products.

Even simple reactions can also lead to the production of "different" daughter nuclides in the form of isomeric states. These isomeric states are long-lived excited states of one and the same nuclide but their behaviour can be quite different. The following reactions are a good example of why this distinction is important:

$$^{241}\text{Am} + \text{n} \rightarrow {}^{242g}\text{Am} + \gamma \tag{2.1}$$

$$^{241}\text{Am} + \text{n} \rightarrow {}^{242m}\text{Am} + \gamma \tag{2.2}$$

Even though ^{242g}Am and ^{242m}Am are essentially the same nuclide, they lead to very different transmutation paths. ^{242}Am in the ground state has a half-life of 16 hours and will therefore decay almost immediately to ^{242}Cm via β^--decay and then to ^{238}Pu via α-decay whereas ^{242m}Am (the isomeric state with a half-life of 142 years) can be transmuted into higher Am and Cm isotopes such as for instance in ^{243}Am and ^{244}Cm.

To take such isomeric states into account during the irradiation of a material, a depletion code needs the proper isomeric branching ratio λ_s for every isomeric state *s* produced in a reaction. This isomeric branching ratio of an isomeric state for a given reaction is defined as the fraction of that isomeric state produced for every occurrence of that reaction.

The composition of certain actinides such as ^{238}Pu and some Cm isotopes are quite sensitive to the value of the isomeric branching ratio for the previously mentioned ^{241}Am neutron capture reaction. This influence is well illustrated in figure 2.1. This figure shows the relative difference with experimental data for all actinides measured for a PWR UO_2 fuel pin when using different constant values (respectively 80, 85 and 90 %) for the ^{241}Am neutron capture branching ratio towards ^{242g}Am.

The impact of changing the branching ratio is very "localised", we only observe a visible influence on ^{238}Pu, ^{242m}Am, ^{242}Cm and ^{243}Cm. The most significant effect is obviously observed for ^{242m}Am. With a branching ratio of 80 % towards ^{242g}Am (i.e. 20 % towards ^{242m}Am), we obtain on overestimation of ^{242m}Am content by about 85 % compared to the experimental value. When increasing the $^{241}\text{Am}(\text{n},\gamma)^{242g}$Am branching ratio to 85 and 90 % (which means that the production of ^{242m}Am is respectively reduced by 1/4 and 1/2 compared to the initial value), the difference with the experimental result for ^{242m}Am is respectively reduced to an overestimation of about 40 % and an underestimation of about 10 %.

The increase of the $^{241}\text{Am}(\text{n},\gamma)^{242g}$Am branching ratio from 80 to 90 % increases the ^{242g}Am production by (only) 12.5 %. As such, the impact on the transmutation chains around this nuclide will be less significant. The prediction of the ^{242}Cm and ^{243}Cm content improves for instance by about 5 to 10 % while the ^{238}Pu content prediction improves by only a few percent. More examples of the impact of this branching ratio value can be found in the work of Golyand et al [1] (which illustrates the impact on the effective multiplication factor and the concentration of

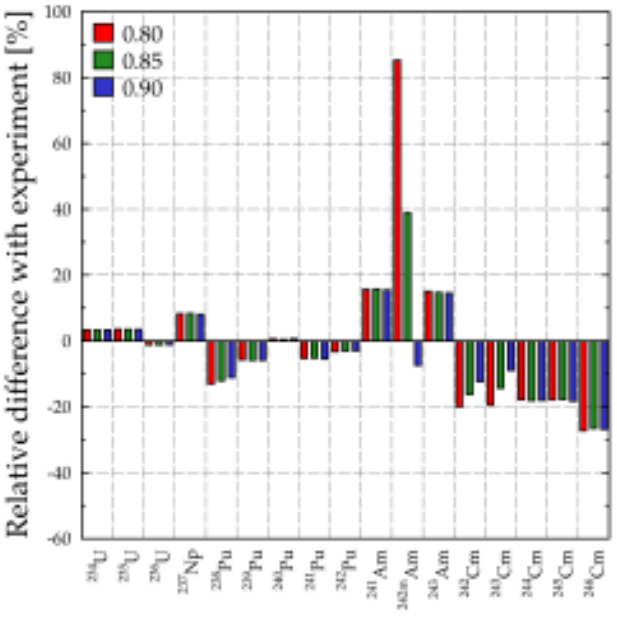

Figure 2.1: The influence of the isomeric branching ratio for the ^{241}Am(n,γ)^{242g}Am reaction on actinide compositions in a PWR UO_2 fuel pin.

several Pu, Am and Cm isotopes as a function of time) and Botazolli et al [2] (on the influence of the ^{241}Am(n,γ)^{242g}Am branching ratio on the helium production in MOX fuel).

To improve the prediction of nuclide compositions for this example and other similar cases, a burn up dependent isomeric branching ratio treatment in which the isomeric branching ratios are evaluated at every time step during the depletion calculation using evaluated nuclear data has been implemented in VESTA. More information along with validation results using experimental data can be found in [3, 4].

2.2 A general burn up dependent treatment

The time dependence of atomic densities when a material is subjected to radiation or when it decays is described by the Bateman equations, a set of coupled linear differential equations. In order to simplify the time dependence, any depletion code will iterate between a steady state transport calculation (which uses either deterministic or stochastic methods) and a zone by zone material evolution through the Bateman equations. In this case, the material compositions in every one of those zones are considered spatially constant when determining the particle flux in the steady state transport calculation and the particle flux (and the associated spectrum) is assumed to be constant in space and time during a time step in the evolution calculation (it should be noted that some of the predictor-corrector algorithms employed by depletion codes sometimes develop the flux and the neutron spectrum over a time step as a linear interpolation or other lower order polynomial). When taking all this into account, the Bateman equations for a particular nuclide *i* can be written as follows after integration over a single depletion zone:

$$\frac{d}{dt} n_i(t) = \sum_j B_{ij}(t)\, n_j(t) \tag{2.3}$$

where B_{ij} is an element of the transition matrix of the Bateman equations for the time step:

$$B_{ij}(t) = \begin{cases} L_{ij}\lambda_j + \sum_r Y_{ij,r}(t)\,\sigma_{j,r}(t)\,\phi(t) & \text{for } i \neq j \\ -\lambda_i - \sum_r \sigma_{i,r}(t)\,\phi(t) & \text{for } i = j \end{cases} \quad (2.4)$$

in which:
- n_i is the atomic density of nuclide i;
- λ_i is the total decay constant of nuclide i;
- L_{ij} is the decay branching ratio of nuclide j to nuclide i (the fraction of all disintegrations of nuclide j that results in the creation of nuclide i);
- $Y_{ij,r}$ is the yield of nuclide i for reaction r on nuclide j (the amount of nuclide i created in a single reaction r on nuclide j):

$$Y_{ij,r}(t) = \frac{\int\int Y_{ij,r}(E)\,\sigma_{j,r}(E)\,\phi(\mathbf{r},E,t)\,dEdV}{\int\int \sigma_{j,r}(E)\,\phi(\mathbf{r},E,t)\,dEdV} \quad (2.5)$$

- $\sigma_{i,r}$ is the microscopic cross section of nuclide i for a reaction r:

$$\sigma_{i,r}(t) = \frac{\int\int \sigma_{i,r}(E)\,\phi(\mathbf{r},E,t)\,dEdV}{\int\int \phi(\mathbf{r},E,t)\,dEdV} \quad (2.6)$$

- ϕ is the scalar particle flux:

$$\phi(t) = \frac{\int\int \phi(\mathbf{r},E,t)\,dEdV}{\int dV} \quad (2.7)$$

For nearly all neutron induced reactions the one group yields $Y_{ij,r}$ defined by equation 2.5 will be equal to one. One exception to this fact is obviously the fission reaction (where the yields $Y_{ij,r}$ actually represent the fission product yields), but there are also those reactions that can produce nuclides in various isomeric states for which the yields $Y_{ij,r}$ represent the isomeric branching ratios $\lambda^s_{j,r}$. As shown in the introduction, neutron capture on ^{241}Am is a well known example.

Ideally, the burn up zones over which the Bateman equations are solved should properly account for the spatial dependence of the neutron flux in a reactor. This is also the case for the time steps to take into account the changes in the neutron spectrum during irradiation. Fissions products such as ^{135}Xe and ^{149}Sm will act as a neutron poison which will have its impact on the neutron spectrum. On the other hand, neutron capture on a fertile material such as ^{238}U will ultimately result in the creation of fissile nuclides such as ^{239}Pu and ^{241}Pu. During irradiation, the importance of those created fissile nuclides will increase as the original fissile material is depleted, resulting in significant spectral changes because the cross sections of those nuclides are distinctly different. All this results in a dependence on time and burn up of the values of the spectral and spatial averaged quantities defined by equation 2.5 to 2.7.

Equation 2.5 gives a constant value for the entire irradiation history only if the yield $Y_{ij,r}$ is an energy independent quantity. This is not the case for the isomeric branching ratio $\lambda^s_{j,r}$ because the isomeric branching ratio data available in nuclear data libraries clearly exhibits a dependence on the incident neutron energy. Furthermore, this energy dependence of isomeric branching ratio data is often not well known. This is nicely illustrated in figure 2.2 which shows the ^{241}Am (n,γ) branching ratio towards the ^{242}Am ground state from the ENDF/B-VII.0 [8], JEFF 3.1 [9]

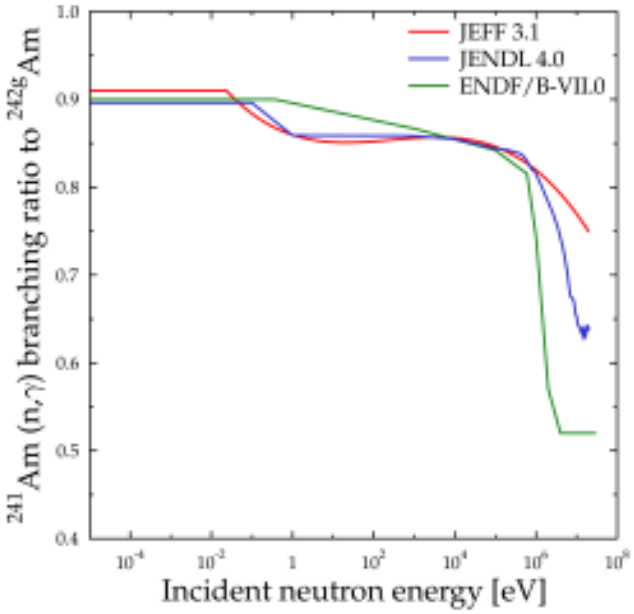

Figure 2.2: The ^{241}Am (n,γ) branching ratio towards the ^{242}Am ground state from the JEFF 3.1, ENDF/B-VII.0 and JENDL 4.0 nuclear data libraries.

and JENDL 4.0 [10] evaluated nuclear data libraries and by the work of Talou et al [11]. Below 1 eV, all three libraries are in good agreement (about 90 % of all (n,γ) interactions with ^{241}Am go to the ^{242}Am ground state) as well as between 10 keV and 1 MeV. From that point on, the library values start to differ. The branching ratio from the JEFF 3.1 nuclear data libary remains roughly the same and does not drop below 75 % while the JENDL 4.0 and ENDF/B-VII.0 nuclear data library continue to drop to a value of respectively 65 and 50 % above 1 MeV. In thermal systems these differences at high energy in the various libraries will have little influence, but in fast spectrum systems this probably will not be the case, as has already been illustrated by Golyand et al [1].

As far as we know, practically all existing depletion codes only evaluate equations 2.6 and 2.7 as a function of the irradiation history while they use constant burn up independent values for the fission yield data and isomeric branching ratio data taken from problem dependent libraries. In this case, the isomeric branching ratios are evaluated for specific systems using equation 2.5 to take into account the effect of the neutron spectrum of the system on the isomeric branching ratio. However, this is only done for a single point in time and the resulting value is used over the entire irradiation history. This also implies that a user has to make a motivated choice of which problem dependent library applies the most to his application which in some cases can be quite difficult. Golyand et al [1] show this process of branching ratio evaluation for ^{241}Am neutron capture and the subsequent variation of this branching ratio for a number of configurations.

This also applies to the current release of VESTA which reads fission yield data from ENDF files and the isomeric branching ratio data from existing problem dependent ORIGEN 2.2 data libraries. An exception that we know of is the APOLLO 2.8 code [7] developed by CEA (France) which has a burn up dependent branching ratio treatment for at least ^{241}Am.

It is now clear that, from a physics point of view, the use of a single constant value for the isomeric branching ratio over the entire irradiation history might not be entirely correct. One way to solve this (and similar issues on other isotopes with neutron induced reactions that involve the production of isomeric nuclides) is to provide a general burn up dependent treatment to estimate the branching ratio using the available energy dependent data for every time step in the irradiation history.

At this point, it is also interesting to note that this approach can be applied to direct fission yield data as well. Like any other nuclear data property, the fission product yields have some energy dependence. The Evaluated Nuclear Data File (or ENDF) format has therefore foreseen the possibility of adding energy dependent fission product yields as tabulated values, just like a cross section, but with a fixed linear-linear interpolation scheme. The ENDF format states that the energy range over which the yields are given must be the same as the energy range of the fission cross section as it is defined in the cross section data of the ENDF file. Unfortunately this does not appear to be the case, even in the latest evaluated nuclear data libraries (like JEFF 3.1 or ENDF/B-VII.0). In practice, fission yield data are given only for a maximum of 3 incident neutron energies: 0.0253 eV (thermal spectrum fission yields), 400 or 500 keV (fast spectrum fission yields) and 14 MeV (fusion spectrum fission yields). However, it is not advised to use these sets as energy dependent yields using the lin-lin interpolation scheme available in the ENDF format. For the moment, a user should choose a specific set of fission product yields and stick with it. Whenever true energy dependent fission yield data becomes available, the methodology for the isomeric branching ratio data presented in this paper could be adapted to obtain a burn up dependent fission yield data treatment as well.

2.3 Implementation in VESTA

2.3.1 Nuclear data treatment

Depletion codes generally require various types of nuclear data, being the various reaction cross sections (which forms the bulk of the data needed), direct fission product yield data, the total recoverable energy per fission and even decay data. For VESTA, the choice was made to use nuclear data which can be found in Evaluated Nuclear Data Files (or ENDF files) [12] as often as possible. This approach will also allow us to quickly change our data when newer (and better) evaluations become available, making VESTA very flexible in its use of nuclear data.

The current version of VESTA is already capable of using ENDF formatted cross section data, fission yield and decay data. With the present paper, we extend this ENDF compatibility to isomeric branching ratio data as well because the basic ENDF files also contain the required energy dependent information that can be used to estimate the isomeric branching ratios. Within the ENDF format, this data can be given either as multiplicities for radioactive nuclide production (in the ENDF format these are referred to as MF9 or file 9 data) or as cross sections for radioactive nuclide production (in the ENDF format these are referred to as MF10 or file 10 data).

The difference between both files is that file 9 actually gives the energy dependent branching ratio $\lambda^s_{j,r}$ towards a particular excited state s, defined as the ratio of the cross section $\sigma^s_{j,r}$ towards the excited state s to the total reaction cross section $\sigma_{j,r}$:

$$\lambda^s_{j,r}(E) = \frac{\sigma^s_{j,r}(E)}{\sum_s \sigma^s_{j,r}(E)} = \frac{\sigma^s_{j,r}(E)}{\sigma_{j,r}(E)} \tag{2.8}$$

File 10 on the other hand gives the individual cross section $\sigma^{s}_{j,r}$ towards the particular excited state *s* directly. The proper branching ratio can then be determined easily with the previous formula. A reaction that has resonance parameters (such as the (n,γ) reaction) may not use file 10 to represent the different cross sections to the individual isomeric states because the size of file 10 data is limited by the format. Only file 9 may be used for these reactions. Using this file 9 and file 10 data as a basis, it is possible to calculate the isomeric branching ratios $\lambda^{s}_{j,r}$ for every time step and for every nuclide and reaction for which data is available.

Some additional nuclear data processing is however required to use some of these data with VESTA. Up to now, we have been using NJOY [13] to process and linearize the basic ENDF files into point-wise ENDF (also known as PENDF) files usable by VESTA which are then formatted into the corresponding ACE files required by MCNP(X) for transport calculations.

During this process, NJOY actually linearizes file 10 data and adds it to the PENDF files, but it does not add it to the ACE files. File 9 data on the other hand is not treated by NJOY altogether. We therefore created a separate tool to add the file 9 data to the PENDF files produced by NJOY. This allows VESTA access to both types of data (some internal processing is still required to linearize file 9 data before it can be used). VESTA could have been adapted to read both the basic ENDF and processed PENDF files. This last solution was however discarded in favour of modifying the PENDF files because it does not increase the number of files to be read by VESTA.

Because the ACE format is a proprietary format of MCNP(X), neither file 9 or file 10 data can be added to these files. Even if we would be allowed to introduce these data into the ACE format, changes to the MCNP(X) source code would have to be made to both read and use them as input data for tallies in a calculation. We can however use other ways to introduce these data into an MCNP(X) calculation without having to modify the source code, although there are some restrictions (see section 2.3.3).

File 9 and 10 data are however still relatively “rare” in the various evaluated nuclear data libraries that exist. It is therefore still required to use ORIGEN 2.2 libraries as base input for reactions that are known to produce nuclides in different isomeric states when no evaluated isomeric branching ratio exists.

2.3.2 Using the multi-group binning approach

With the development of VESTA, the emphasis has always been on both accuracy and performance because continuous energy Monte Carlo depletion codes have always been known to be very time consuming. It has been shown before [14, 15] that this is mainly due to the calculation of all the cross section values during the Monte Carlo simulation for the evaluation of equation 2.6 for every nuclide and reaction of interest. VESTA solves this problem by offering the use of the multi-group binning approach [14–16] to calculate these reaction rates as an alternative to using the traditional Monte Carlo estimators.

By definition, the integrals given by equation 2.6 and 2.7 can also be calculated as a sum over infinitely small energy intervals:

$$\sigma_{i,r}(t) = \frac{\int\int \sigma_{i,r}(E)\,\phi(\mathbf{r},E,t)\,dEdV}{\int\int \phi(\mathbf{r},E,t)\,dEdV} = \frac{\lim\limits_{g\to\infty}\sum\limits_{g}\sigma^{g}_{i,r}\phi_{g}}{\lim\limits_{g\to\infty}\sum\limits_{g}\phi_{g}} \tag{2.9}$$

$$\phi(t) = \frac{\int\int \phi(r, E, t)\, dE dV}{\int dV} = \frac{\lim_{g\to\infty} \sum_g \phi_g}{\int dV} \tag{2.10}$$

in which $\sigma^g_{i,r}$ and ϕ_g are the average cross section and the spectrum of the energy interval g with boundaries E_{g-1} and E_g:

$$\sigma^g_{i,r} = \frac{\int_{E_{g-1}}^{E_g} \sigma_{i,r}(E)\, dE}{E_g - E_{g-1}} \tag{2.11}$$

$$\phi_g = \int_{E_{g-1}}^{E_g} \phi(E)\, dE \tag{2.12}$$

with $\sigma_{i,r}(E)$ the energy dependent microscopic cross section of the material for which we calculate the reaction rate and $\phi(E)$ the energy dependent spectrum within the burn up zone. Because the energy intervals are infinitely small, there is also no need to use a weighting spectrum for the multi-group cross section (as would be the case for a low number of groups) since the fine group structure is perfectly capable of representing the individual resonances.

This approach of calculating the integrals is exact but to make this approach work numerically a finite number of intervals is required. Fortunately, it is always possible to select an energy structure for these intervals so that the estimate of the single group cross section given by equation 2.9 differs only by an amount ϵ from the exact value. Furthermore, this accuracy criterion can be applied regardless of the convergence of the Monte Carlo simulation [14–16]. The default group structure derived for use by VESTA consists of 43000 groups, but this can be changed by the user.

This method is neither an approximation nor is it a true hybrid method (which is a combination of Monte Carlo and deterministic methods) as it does not interfere in any way with the Monte Carlo simulation itself. At its core, it is just another way to calculate an integral. The name of the multi-group binning approach might be a bit misleading as it refers specifically to a well known technique in deterministic codes although the shear scale on which it is applied is entirely different.

With the multi-group binning approach, the calculation time of every depletion step (regardless of the number of reaction rates required) is thus almost reduced to that of the basic Monte-Carlo simulation because only an ultra-fine multi-group spectrum has to be calculated by the Monte-Carlo code. Due to the very nature of this ultra-fine spectrum, this method takes into account the self-shielding effects due to the resolved resonance range. The reduction in calculation time is quite significant. In practical applications, a speed-up of at least a factor 5 to 10 has been observed [14–16].

This method can now easily be extended to the calculation of the isomeric branching ratios $\lambda^s_{j,r}$ using either file 9 or file 10 data. The way this is done depends on where the data comes from. When the branching ratio data is read from file 9, the average branching ratio $\lambda^s_{j,r}$ can be calculated using an equation which is similar to equation 2.9:

$$\lambda^s_{j,r} = \frac{\int\int \lambda^s_{j,r}(E)\, \sigma_{j,r}(E)\, \phi(r, E, t)\, dE dV}{\int\int \sigma_{j,r}(E)\, \phi(r, E, t)\, dE dV} = \frac{\lim_{g\to\infty} \sum_g \lambda^{g,s}_{j,r} \sigma^g_{j,r} \phi^g}{\lim_{g\to\infty} \sum_g \sigma^g_{j,r} \phi^g} \tag{2.13}$$

with $\sigma_{j,r}^{g}$ the cross section of energy interval g calculated with equation 2.11 and $\lambda_{j,r}^{g,s}$ the branching ratio for energy interval g calculated by:

$$\lambda_{j,r}^{g,s} = \frac{\int_{E_{g-1}}^{E_g} \lambda_{j,r}^{s}(E)\,\sigma_{j,r}(E)\,dE}{\int_{E_{g-1}}^{E_g} \sigma_{j,r}(E)\,dE} \tag{2.14}$$

With file 10 data, the single group cross sections $\sigma_{j,r}^{s}$ towards every particular excited state s can be directly determined using equation 2.9 to obtain the average branching ratio $\lambda_{j,r}^{s}$:

$$\lambda_{j,r}^{s} = \frac{\sigma_{j,r}^{s}}{\sum_{s}\sigma_{j,r}^{s}} = \frac{\sigma_{j,r}^{s}}{\sigma_{j,r}} \tag{2.15}$$

2.3.3 Using Monte Carlo estimators

In accordance with the generic nature of VESTA, a user can also choose to use the traditional method of calculating the reaction rates using Monte Carlo estimators. This gives the user an easy way to test the results obtained with the multi-group binning approach.

The result of a Monte Carlo transport simulation is a set of interaction points with in between particle tracks with a track length l_t, energy E_t and their corresponding weight w_t. Expected values of parameters such as particle flux, current, etc. can be tallied from this set of interaction points and tracks using various types of estimators, either on demand of the user or for use by the code itself. When using the track length estimator (which is the most common Monte Carlo estimator), these parameters can be described using the following integral:

$$\int\int\int h(\mathbf{r}, E, \Omega)\,\varphi(\mathbf{r}, E, \Omega)\,dE d\Omega dV = \frac{1}{W}\sum_{t} l_t w_t h(\mathbf{r}_t, E_t, \Omega_t) \tag{2.16}$$

where h is the response function needed to determine the quantity the user is interested in.

For Monte Carlo burn-up applications, we are mostly interested in estimating the integrals in equations 2.6 and 2.7. The numerator in equation 2.6 is the volume averaged reaction rate associated with a reaction r on the nuclide of type i through the microscopic cross section $\sigma_{i,r}$. The denominator of this equation and the numerator of equation 2.7 is the volume averaged total scalar flux. The response function needed for these integrals will therefore be the reaction cross section $\sigma_{i,r}$ and a unity function. A Monte Carlo code that uses the track length estimator will thus estimate the reaction rate and the total flux as:

$$\int\int \sigma_{i,r}(E)\,\phi(\mathbf{r}, E)\,dE dV = \frac{1}{W}\sum_{t} l_t w_t \sigma_{i,r}(E_t) \tag{2.17}$$

$$\int\int \phi(\mathbf{r}, E)\,dE dV = \frac{1}{W}\sum_{t} l_t w_t \tag{2.18}$$

As a result, the Monte Carlo estimators for equations 2.6 and 2.7 will therefore be given by:

$$\sigma_{i,r}(t) = \frac{\int\int \sigma_{i,r}(E)\,\phi(\boldsymbol{r},E,t)\,dEdV}{\int\int \phi(\boldsymbol{r},E,t)\,dEdV} = \frac{\sum_t l_t w_t \sigma_{i,r}(E_t)}{\sum_t l_t w_t} \tag{2.19}$$

$$\phi(t) = \frac{\int\int \phi(\boldsymbol{r},E,t)\,dEdV}{\int dV} = \frac{1}{W}\frac{\sum_t l_t w_t}{\int dV} \tag{2.20}$$

The extension to burn up dependent isomeric branching ratio data is a bit more tricky. As with the multi-group binning approach, the way this is done depends on the source of the data. For file 9 branching ratio data, the average branching ratio $\lambda^s_{j,r}$ (see equation 2.13) requires the calculation of two integrals. The denominator of this equation is calculated by using equation 2.17. The numerator on the other hand is the volume averaged reaction rate associated with a reaction r on the nuclide of type j through the microscopic cross section $\sigma_{j,r}$ weighted by the energy dependent branching ratio $\lambda^s_{j,r}$ towards the excited state s. The response function needed for this integral will therefore be the product of the branching ratio $\lambda^s_{j,r}$ and the cross section $\sigma_{j,r}$ so that the track length estimator of this weighted reaction rate will be given by:

$$\int\int \lambda^s_{j,r}(E)\,\sigma_{j,r}(E)\,\phi(\boldsymbol{r},E,t)\,dEdV = \sum_t l_t w_t \lambda^s_{j,r}(E_t)\,\sigma_{j,r}(E_t) \tag{2.21}$$

The Monte Carlo estimator for equation 2.13 will therefore be given by:

$$\lambda^s_{j,r} = \frac{\int\int \lambda^s_{j,r}(E)\,\sigma_{j,r}(E)\,\phi(\boldsymbol{r},E,t)\,dEdV}{\int\int \sigma_{j,r}(E)\,\phi(\boldsymbol{r},E,t)\,dEdV} = \frac{\sum_t l_t w_t \lambda^s_{j,r}(E_t)\,\sigma_{j,r}(E_t)}{\sum_t l_t w_t \sigma_{j,r}(E_t)} \tag{2.22}$$

As with the multi-group binning approach, the average isomeric branching ratio is calculated with equation 2.15 when using file 10 data. In this case no additional estimators need to be defined because the single group cross sections $\sigma^s_{j,r}$ towards every particular excited state s can be calculated using the Monte Carlo estimator given in equation 2.19 in which the response function is the energy dependent partial cross section $\sigma^s_{j,r}$.

Three physical quantities represented by the integrals given in equations 2.17, 2.18 and 2.21 have to be estimated to obtain all the data we need for the depletion calculation. When using a Monte Carlo code such as MCNP(X) as the transport module in VESTA, the calculation of these quantities is reduced to specifying a track length tally (an f4 type tally in MCNP(X) jargon) in all the cells corresponding to the various depletion zones.

No additional effort is required for the estimation of the total flux given by equation 2.18. To calculate the reaction rate given by equation 2.17, the track length tally must be combined with a cross section response function (for every reaction and nuclide considered in the evolution chains). With MCNP(X), this is achieved by using a tally multiplier (an fm multiplier in MCNP jargon). This requires the reaction data to be given in the ACE files.

When using file 9 branching ratio data, the denominator of equation 2.22 corresponds to values that were already calculated using the previously described track length tally combined with the proper fm multiplier. The calculation of the weighted reaction rate in the numerator of this equation requires the introduction of a weighting function (the energy dependent branching ratio) and a cross section as a response function in the track length tally. As usual, a tally multiplier is used for the cross section. A dose function or detector response function (a de/df dose function in MCNP(X) jargon) is used to specify the linearised file 9 data for a single isomeric state. Because an MCNP(X) tally can only have a single dose function associated to it, it is necessary to add as many tallies as there are reactions and isomeric states for which we need to evaluate the average branching ratio $\lambda^s_{j,r}$.

When using file 10 data, we need to calculate equation 2.19 using the partial cross section $\sigma^s_{j,r}$ towards every particular excited state *s* as a response function to obtain the average branching ratio value. These cannot be estimated using the traditional tally multiplier within MCNP(X) because those partial cross sections are not available in the ACE files. Instead, they can be calculated using yet another track length tally in combination with a de/df dose function (no tally multipier is used in this case). The de/df dose function is used to specify the linearised partial cross section towards a single excited state. As with the file 9 data, it is required to add as many tallies as there are partial cross sections in the file 10 data.

This implementation requires the addition of a large number of tallies with corresponding dose functions (using the available file 9 and 10 data) to the input file. The number of dose functions that can be specified in MCNP(X) is however limited to about 100. For our applications (in which we only take into account isomeric production for neutron capture and the n,2n reaction because ORIGEN 2.2 libraries only take into account isomeric production for these reactions), this is not a limiting factor but it might become one when we wish to use isomeric branching ratio data for other reactions.

All the tallies described here are automatically added by VESTA to the MCNP input file (depending on the nuclear data specified by the user). No direct intervention by the user is therefore required.

2.3.4 Validation of the implementation

First of all, we have to show that the branching ratios calculated with the multigroup binning approach and the Monte Carlo estimators are equivalent. This approach of calculating the integrals using equations 2.9, 2.10 and 2.13 is exact, but to make this approach work numerically, we will need a finite number of energy intervals. In addition, the actual difference between both methods must be independent of the convergence of the Monte Carlo simulation. Otherwise it would not make much sense to use a new method that accelerates one part the calculation and on the other hand looses what was gained because it needs more precision for it to work. Such a group structure using 43000 groups has been derived and validated in the past for equations 2.9 and 2.10 [14–16]. There is no need in adapting this default group structure when applying it to branching ratio data because the branching ratio data is a lot “smoother” compared to the reaction cross sections themselves, as evidenced in figure 2.2.

We have calculated the values for the branching ratios to the ground state for some nuclides that have file 9 or 10 data in the JEFF 3.1 nuclear data library for the GGU2 fuel sample already mentioned in the introduction. The results as a function of the convergence of the Monte Carlo simulation can be found in table 2.1. It is clear from the values in this table that the multigroup binning approach gives values well within the relative error of the Monte Carlo values. The

relative difference between both values is more important for the high energy reactions due to the fact that the Monte Carlo simulation uses probability tables in the unresolved energy range which cannot be taken into account with the multigroup binning approach. If we switch off the probability tables, the agreement improves to the level of the other reactions. Because the probability tables are important for the correct simulation of neutron transport in the unresolved resonance energy range, we prefer to keep them switched on for our simulations.

Table 2.1: Isomeric branching ratio values to the ground state and relative errors (in %) calculated using Monte Carlo estimators and the multigroup binning approach for a PWR UO2 fuel pin at BOL using the JEFF 3.1 nuclear data library.

Nuclide	^{76}Ge	^{76}Ge	^{103}Rh	^{103}Rh	^{129}I	^{204}Pb	^{209}Bi	^{237}Np	^{241}Am
Reaction	(n,2n)	(n,γ)	(n,2n)	(n,γ)	(n,γ)	(n,2n)	(n,γ)	(n,2n)	(n,γ)
File	10	9	10	10	10	10	9	9	9
PWRU50.LIB	-	61.99	100.00	93.01	62.53	100.00	57.58	25.85	80.00
n/cycle	Calculated branching ratios (in %) using Monte Carlo estimators								
5000	41.35	32.83	61.29	95.66	57.22	76.50	79.48	25.05	87.26
20000	40.91	32.85	60.53	95.66	57.23	75.09	79.58	25.05	87.25
40000	41.02	32.84	60.91	95.67	57.22	75.80	79.58	25.06	87.25
80000	41.06	32.84	60.81	95.67	57.22	75.83	79.55	25.06	87.25
100000	41.08	32.82	60.91	95.67	57.22	75.98	79.54	25.06	87.25
n/cycle	Calculated branching ratios (in %) using the multigroup binning approach								
5000	41.18	32.88	61.07	95.67	57.22	75.91	79.65	25.07	87.25
20000	41.19	32.86	61.15	95.66	57.22	76.51	79.54	25.07	87.25
40000	41.21	32.83	61.01	95.67	57.22	76.20	79.54	25.07	87.25
80000	41.11	32.86	60.87	95.67	57.22	75.72	79.55	25.07	87.25
100000	41.02	32.85	60.79	95.67	57.22	75.70	79.53	25.07	87.25
n/cycle	Relative error (in %) on the branching ratios using Monte Carlo estimators								
5000	14.540	9.594	14.141	0.497	0.509	10.669	3.815	4.927	0.841
20000	6.914	4.567	6.666	0.239	0.264	5.187	2.083	2.447	0.420
40000	4.468	3.180	4.334	0.179	0.184	3.428	1.461	1.720	0.300
80000	3.211	2.274	3.103	0.120	0.124	2.419	1.031	1.200	0.201
100000	2.885	2.047	2.775	0.119	0.120	2.161	0.915	1.060	0.181
n/cycle	Relative difference (in %) between the branching ratios estimated using Monte Carlo estimators and the multigroup binning approach								
5000	0.419	0.176	0.359	0.006	0.005	0.766	0.221	0.080	0.013
20000	0.699	0.017	1.018	0.001	0.005	1.893	0.054	0.074	0.000
40000	0.485	0.015	0.151	0.003	0.006	0.521	0.043	0.053	0.001
80000	0.129	0.057	0.097	0.001	0.001	0.147	0.005	0.051	0.001
100000	0.162	0.086	0.203	0.001	0.001	0.379	0.006	0.058	0.001

2.3.5 Comparison with ORIGEN library values

Table 2.1 also gives the values of the corresponding branching ratio from the PWRU50.LIB activation library of ORIGEN 2.2 which has been used as a base library for the GGU2 simulation. The comparison of these values with those calculated using JEFF 3.1 data illustrates why the reevaluation of the isomeric branching ratio could be important. The PWRU50.LIB library does

not even have a value for the (n,2n) reaction of ^{76}Ge altogether so no value can be given for this branching ratio. Furthermore, for the (n,2n) reaction on ^{103}Rh and ^{204}Pb we see that ORIGEN 2.2 did not even make a distinction in the production of the reaction product in the ground state and a metastable state (hence the branching ratio of 100 % for those nuclides and reactions). For neutron capture on ^{76}Ge and ^{209}Bi, the evaluated values are very different of the original values. In all other cases, the calculated branching ratios are roughly of the same order of magnitude as the ORIGEN 2.2 values. The calculated value of the ^{241}Am (n,γ) branching ratio towards ^{242g}Am is for instance 87.25 % while the ORIGEN 2.2 value was 80 %. As we have shown in section 2.1, this change will definitely have a significant impact on the composition of several actinides.

3 MODELLING HFR-EU1

3.1 The HFR-EU1 experiment

The HFR-EU1 irradiation experiment in the High Flux Reactor (HFR) in Petten was proposed in 2002 to the European High Temperature Reactor Technology Network (HTR-TN) and to the Institute of Nuclear and New Energy Technology (INET, China) to compare the performance of historical and newly produced fuel and to provide high burn-up pebbles for safety testing. The experiment consists in the irradiation of 5 complete HTR fuel pebbles designated HFR-EU1/1 to HFR-EU1/5 and a number of smaller capsules containing a small number of TRISO particles. HFR-EU1/1 and HFR-EU1/2 are 2 Chinese HTR-10 pebbles produced by INET while HFR-EU1/3 to HFR-EU1/5 are 3 German AVR GLE-4 pebbles manufactured by HOBEG in October 1987. The main characteristics of these two pebble types is given in Table 3.2. HFR-EU1 was designed to reflect realistic operating conditions of the HTR fuel pebbles (i.e. realistic fuel temperatures) up to high burn up.

The irradiation campaign was integrated in the now completed Euratom projects HTR-F/F1 and RAPHAEL related to R&D on the innovation potential of past and current HTR fuel technology based on TRISO coated particles. The current ARCHER project covers the post-irradiation examination of the irradiated AVR fuel pebbles HFR-EU1/3 to HFR-EU1/5.

The Chinese and German fuel pebbles were physically separated from each other in the irradiation rig. The Chinese pebbles HFR-EU1/1 and HFR-EU1/2 were placed in a dedicated capsule at the top of the irradiation rig while the German spheres HFR-EU1/3 to HFR-EU1/5 were placed in a separate capsule placed under the Chinese capsule. The entire irradiation rig was connected to a gas handling facility to enable continuous fission gas release analysis. Both capsules were equiped with instrumentation for the measurement of the operating temperature and the accumulated neutron fluence.

The irradiation of the fuel spheres was performed in two campaigns from September 29, 2006 to February 24, 2008 (12 reactor cycles of 28 days each) and continued from October 19, 2009 to February 19, 2010 (4 reactor cycles) for a total of 445 effective full power days. The interruption of the irradiation by 1.5 years was imposed partly by reactor outage and partly by an unexpected thermocouple failure in one of the capsules. The irradiation rig was placed in three different positions for each campaign (see Figure 3.1): position H2 for the first campaign, position H4 for the second campaign and F2 for the third and final campaign. Table 3.1 gives the irradiation history of the HFR-EU1 iradiation rig along with representative thermal flux levels [17, 18, 20].

The information given in this chapter is limited to what is relevant for the irradiation and depletion modelling with the VESTA software. For additional information on the HFR-EU1 experiment we refer to references [17] and [18]. All data given in this chapter come from publicly available sources unless stated otherwise.

3.2 Initial material compositions

The data given in Table 3.2 allows us to calculate the initial composition of the UO_2 fuel kernel of an INET and AVR fuel pebble. The resulting compositions are given in Table 3.3.

For both fuel pebbles, we know the initial ^{235}U enrichment e_{U235} (given in weight fraction) and the total initial ^{235}U content c_{U235} (given in grams per pebble). The total heavy metal content

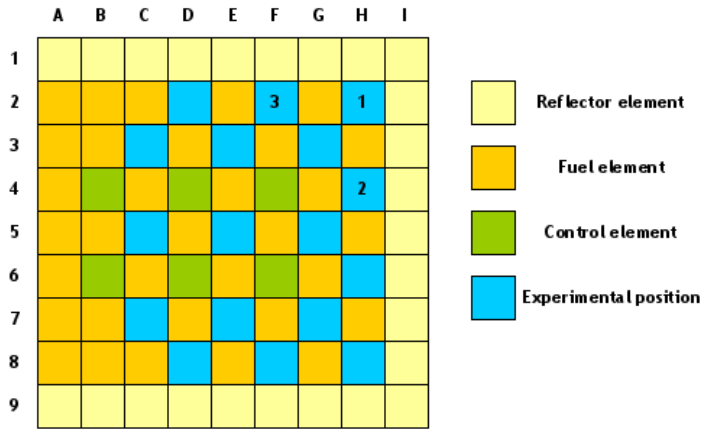

Figure 3.1: The HFR core configuration and the positions of the HFR-EU1 irradiation rig during the irradiation.

c_{HM} (given in grams per pebble) for a single pebble is thus given by:

$$c_{HM} = \frac{c_{U235}}{e_{U235}} \tag{3.1}$$

The ratio of the heavy metal content c_{HM} to the total oxide content c_{UO2} (given in grams per pebble) can be calculated as follows:

$$\frac{c_{HM}}{c_{UO2}} = \frac{1}{2A_{O16}\left(\frac{e_{U235}}{A_{U235}} + \frac{1-e_{U235}}{A_{U238}}\right)} \tag{3.2}$$

in which A_{U235}, A_{U238} and A_{O16} respectively represent the atomic mass of ^{235}U, ^{238}U and ^{16}O. Please note that we assume that there is no ^{234}U or ^{236}U present in the fuel (even though there will be some trace amounts present). This approximation will have a direct influence on the final compositions of these nuclides but also indirectly on the composition of some nuclides such as ^{237}Np and ^{238}Pu.

Using the total heavy metal content c_{HM} and the atomic mass values, we can use the previous formula to calculate the total oxide content c_{UO2}. The fuel density ρ (given in g cm^{-3}) is then given by:

$$\rho = \frac{c_{UO2}}{NV} \tag{3.3}$$

where N is the number of TRISO particles and V is the volume of a single fuel kernel inside the sphere. Using the data from Table 3.2, we thus obtain densities of respectively 10.87 and 10.69 g cm^{-3} for an INET and AVR fuel pebble.

3.3 Neutron spectra

When performing depletion calculations, it is important to properly represent the variation of the neutron spectra to which an irradiated material is subjected. In many depletion codes (including the VESTA software), this is achieved by iterating between a detailed transport calculation (using a geometrical model of the irradiated materials along with its environment) and

Table 3.1: HFR-EU1 irradiation history and reported thermal flux levels.

Cycle	Position	Cooling time [days]	Irradiation time [days]	Thermal flux [10^{14} cm^{-2} s^{-1}]
2006-08	H2	-	24.23	0.697
2006-09	H2	3.86	26.88	0.691
2006-10	H2	3.48	28.56	0.730
2007-01	H4	2.97	27.88	0.866
2007-02	H4	3.09	28.91	0.878
2007-03	H4	24.13	27.85	0.878
2007-07	F2	119.5	27.45	1.110
2007-08	F2	3.29	28.73	1.140
2007-09	F2	3.06	27.99	1.120
2007-10	F2	4.16	27.82	1.070
2008-01	F2	3.2	27.75	1.070
2008-02	F2	3.25	28.72	1.150
2009-08	F2	603.24	24.76	1.100
2009-09	F2	3.59	31.37	1.110
2009-10	F2	3.67	24.32	1.090
2010-01	F2	3.34	31.66	1.090

a depletion calculation of the irradiated materials using flux and reaction rate data from the transport calculation.

From a general point of view, this requires accurate and detailed information on the irradiation conditions and the environment of the irradiated materials. This information is not readily available in the case of the HFR-EU1 experiment due to the confidential nature of some of the irradiation rigs in the vicinity of the HFR-EU1 irradiation rig.

Due to the limited amount of fissile material present in each sphere (which is less than 5 g for all fuel pebbles combined), it is safe to assume that the neutron spectrum that will dominate the irradiation of the pebbles is the spectrum produced around the irradiation rig and that the pebbles themselves will have little to no impact on the spectrum to which they are subjected. It was therefore decided in collaboration with NRG [20] to calculate representative unperturbed neutron spectra for each fuel pebble and for each position of the HFR-EU1 irradiation rig. As a result, no additional data on the environment of the irradiation rig was required to perform the depletion calculations presented in this report.

These ‘unperturbed neutron spectra’ are the spectra that calculated at the exact location of the pebbles in the HFR-EU1 irradiation rig but with the inner 5 cm diameter of the pebbles replaced by a void material (i.e. total abscense of any atom). The unperturbed spectra have been calculated using three MCNP models for specific cycles of the HFR representative of the three positions of the HFR-EU1 irradiation rig, being cycles 2006-09 (position H2 in the first campaign), 2007-02 (position H4 in the second campaign) and 2007-08 (position F2 in the first campaign). These spectra were calculated in the standard 43000 group structure as required by VESTA so that these spectra can be easily transmitted to VESTA for the depletion calculations.

Table 3.2: INET and AVR fuel pebble and particle characteristics [17, 18].

Pebble characteristic	Unit	INET	AVR
Heavy metal loading	g pebble^{-1}	5.02	6.0
^{235}U content	g pebble^{-1}	0.858	1.00 ± 1 %
Number of TRISO particles		8500	9560
Volume packing fraction	%	5.0	6.2
Free U fraction		2.3 10^{-7}	7.8 10^{-6}
Matrix graphite grade		A3-3	A3-3
Matrix density	kg m^{-3}	1760	1750
Temperature at final heat treatment	Celsius	1900	1900
Particle characteristic	**Unit**	**INET**	**AVR GLE4**
Particle batch		V000802	HT 384-393
Kernel composition		UO_2	UO_2
^{235}U enrichment	w%	17.08	16.76
Kernel diameter	μm	490.3	502
Particle diameter	μm	926.9	916
Particle buffer thickness	μm	97	92
Particle inner PyC thickness	μm	42	40
Particle SiC thickness	μm	37.8	35
Particle outer PyC thickness	μm	40.8	40

3.4 Irradiation history

As mentioned in the previous section, the spheres do not have a major impact on the overall neutron spectrum inside the irradiation rig so that the use of unperturbed spectra can be justified. However, the presence of these spheres will however have an impact the absolute flux levels seen by the TRISO particles in each sphere. The calculations of NRG, that provide us with the unperturbed neutron spectra, also give us the absolute unperturbed neutron flux levels at the position of the spheres which we can use to calculate a first estimate of the irradiation history. These flux values can be used as a first estimate of the neutron flux but a correction of those flux levels will be required to obtain the correct burn up of each sphere.

These absolute unperturbed neutron flux levels are only valid for the three HFR reference cycles used for the calculation of the unperturbed neutron spectra (being 2006-09, 2007-02 and 2007-08). To obtain the corresponding absolute flux levels of the other HFR cycles, we can use the relative variation of the flux of a given cycle within each irradiation campaign to the respective reference cycle using the data in Table 3.1.

The resulting flux levels for each fuel sphere are given in Table 3.5 along with the resulting burn up level given in % FIMA. These burn up levels were obtained by calculating the number of fissions of all fissionable actinides over each cycle as follows:

$$\mathrm{BU} = \sum_j \sum_i N_i \sigma_{f,i} \phi_j \Delta t_j \tag{3.4}$$

in which N_i and $\sigma_{f,i}$ are respectively the concentration and microscopic fission cross section of actinide i and where ϕ_j and Δt_j are respectively the total flux level and duration of cycle j.

Table 3.3: Fuel kernel compositions for the INET and AVR fuel pebbles (given in atoms barn^{-1} cm^{-1} and gram cm^{-3}).

	INET kernel		AVR kernel	
Nuclide	atoms barn^{-1} cm^{-1}	gram cm^{-3}	atoms barn^{-1} cm^{-1}	gram cm^{-3}
^{16}O	4.855661E-2	1.28969	4.777412E-2	1.26891
^{235}U	4.190626E-3	1.63563	4.046012E-3	1.57918
^{238}U	2.008768E-2	7.94064	1.984105E-2	7.84315
Total	7.283491E-2	10.87	7.166119E-2	10.69

When comparing these burn up levels with those from Table 3.4, we clearly see that the obtained burn up levels are about 20 to 40 % higher than expected.

Table 3.4: Final burn up levels of the HFR-EU1 fuel spheres.

Sphere	Burn up [% FIMA]
HFR-EU1/1	9.30
HFR-EU1/2	11.60
HFR-EU1/3	13.90
HFR-EU1/4	14.30
HFR-EU1/5	13.50

There are several methods we can use to renormalise these flux levels. The best method is to use burn up indicators or tracers, which are fission products that are known to be characterized by a linear behaviour with respect to burn up (whatever the spectrum conditions might have been nearby the sample). These tracers are often used to bring the calculated irradiation history back to the actually measured burn up level. Nd and Cs isotopes are broadly recognized as accurate burn up indicators, the first of which can be experimentally determined by radiochemistry and the second one through gamma spectrometry.

Several activity measurements were performed on the HFR-EU1/3 and HFR-EU1/4 spheres, including measurements of ^{137}Cs which we have selected as a burn up tracer [19]. For the remaining three spheres (HFR-EU1/1, HFR-EU1/2 and HFR-EU1/5), no experimental data is available so we will normalise the irradiation history for these spheres by using the burn up values as reported by NRG (see Table 3.4).

In all cases, the normalisation consists of determining a global renormalisation constant f_s for each sphere which is applied to the irradiation history as a whole. This renormalisation constant f_s is determined through iteration. For every iteration, a calculation is run using the scaling factor f_s determined in the previous iteration (for the first iteration, this factor is set to 1.000). We calculate the $(C/E)_i$ value for the normalisation parameter (i.e. the ^{137}Cs activity for the HFR-EU1/3 and HFR-EU1/4 spheres and the burn up for the other spheres) for each iteration i and compare it to the target $(C/E)_t$ value (being 1.000 in this case). The relative difference δ of the $(C/E)_i$ value to the target value $(C/E)_t$ is then used to determine the scaling factor for the

Table 3.5: Initial estimate of the absolute neutron flux levels (given in 10^{14} neutrons cm^{-2} s^{-1}) for each sphere taking into account flux variations between cycles. The reference cycle for each campaign is highlighted in bold.

Cycle	HFR-EU1/1	HFR-EU1/2	HFR-EU1/3	HFR-EU1/4	HFR-EU1/5
2006-08	2.26475	2.60090	2.75672	2.68993	2.40903
2006-09	2.24526	2.57852	2.73300	2.66678	2.38830
2006-10	2.37198	2.72406	2.88725	2.81730	2.52309
2007-01	3.22900	3.81219	4.10643	4.06179	3.65228
2007-02	3.27375	3.86503	4.16334	4.11808	3.70290
2007-03	3.27375	3.86503	4.16334	4.11808	3.70290
2007-07	3.87681	4.53430	4.85709	4.77484	4.27791
2007-08	3.98161	4.65687	4.98839	4.90391	4.39355
2007-09	3.91177	4.57519	4.90089	4.81790	4.31649
2007-10	3.73714	4.37094	4.68210	4.60281	4.12379
2008-01	3.73714	4.37094	4.68210	4.60281	4.12379
2008-02	4.01653	4.69771	5.03214	4.94692	4.43208
2009-08	3.84189	4.49346	4.81334	4.73183	4.23938
2009-09	3.87681	4.53430	4.85709	4.77484	4.27791
2009-10	3.80698	4.45262	4.76960	4.68882	4.20085
2010-01	3.80698	4.45262	4.76960	4.68882	4.20085
Burn up [% FIMA]	16.13	18.17	18.9	18.6	17.14

next iteration:

$$\delta = \frac{\left(\frac{C}{E}\right)_i - \left(\frac{C}{E}\right)_t}{\left(\frac{C}{E}\right)_t} \tag{3.5}$$

$$f_s = f_s\,(1-\delta) = f_s\left(1 - \frac{\left(\frac{C}{E}\right)_i - \left(\frac{C}{E}\right)_t}{\left(\frac{C}{E}\right)_t}\right) \tag{3.6}$$

This iteration procedure continues until the relative difference between the $(C/E)_i$ value for the normalisation parameter to the target $(C/E)_t$ value (being 1.000 in this case) is less than 0.1 %.

When using a parameter such as the ^{137}Cs activity for the normalisation of the irradiation history, the measurement uncertainty on normalisation parameter will introduce an uncertainty on the normalisation of the irradiation history. This uncertainty translates to a burn up range for each sphere centered around the burn up value corresponding to the normalised irradiation history. Due to the abscence of an error on the reported burn up levels, we cannot associate an uncertainty to the normalisation for the HFR-EU1/1, HFR-EU1/2 and HFR-EU1/5 spheres.

In order to estimate the uncertainty due to the normalisation for the HFR-EU1/3 and HFR-EU1/4 spheres, we need to determine the C/E value of the ^{137}Cs activity associated with the burn up values corresponding to the boundaries of that burn up range. This is done using the same iterative procedure as described above in which the initial normalisation factor f_s and the target $(C/E)_t$ value for the ^{137}Cs activity are changed. This is done twice, once for the upper value of the burn up range and once for the lower value of the burn up range. The target $(C/E)_t$ value

and initial normalisation factor f_s for this upper and lower boundary of the burn up range are initialised as follows:

$$\left(\frac{C}{E}\right)_t = 1.000 \pm 3\sigma \tag{3.7}$$

$$f_s = f_s\,(1 \pm 3\sigma) \tag{3.8}$$

In these equations, σ is the uncertainty on the ^{137}Cs activity C/E value calculated in the last iteration for the calibration of the irradiation history. To estimate the value of σ, we assume that the relative error on the C/E value equals the relative error on the experimental values for the ^{137}Cs activity.

The final flux levels for each fuel sphere after normalisation are given in Table 3.6 along with the resulting final burn up level (given in % FIMA). As could be expected, these final burn up values are almost equal to the reported burn up levels for the HFR-EU1/1, HFR-EU1/2 and HFR-EU1/5 spheres. For the HFR-EU1/3 and HFR-EU1/4 spheres, the difference between the final burn up value and the reported value are rather large, respectively 6.7 and 3.1 %. These differences are however within the uncertainty of the ^{137}Cs activity measurement. For a detailed discussion, we refer to section 4.2 of the next chapter in which we discuss the results for the HFR-EU1/3 and HFR-EU1/4 spheres in detail.

Table 3.6: Final estimate of the absolute neutron flux levels (given in 10^{14} neutrons cm^{-2} s^{-1}) for each sphere taking into account flux variations between cycles. The reference cycle for each campaign is highlighted in bold.

Cycle	HFR-EU1/1	HFR-EU1/2	HFR-EU1/3	HFR-EU1/4	HFR-EU1/5
Normalisation	burn up	burn up	^{137}Cs activity	^{137}Cs activity	burn up
Factor	0.50458	0.55975	0.72218	0.73166	0.73141
2006-08	1.14275	1.45586	1.99085	1.96811	1.76199
2006-09	1.13291	1.44333	1.97372	1.95118	1.74682
2006-10	1.19686	1.52479	2.08511	2.06130	1.84542
2007-01	1.62929	2.13387	2.96558	2.97185	2.67132
2007-02	1.65187	2.16345	3.00668	3.01304	2.70834
2007-03	1.65187	2.16345	3.00668	3.01304	2.70834
2007-07	1.95616	2.53808	3.50770	3.49356	3.12891
2007-08	2.00904	2.60668	3.60251	3.58800	3.21349
2007-09	1.97380	2.56096	3.53933	3.52506	3.15712
2007-10	1.88569	2.44663	3.38132	3.36769	3.01618
2008-01	1.88569	2.44663	3.38132	3.36769	3.01618
2008-02	2.02666	2.62954	3.63411	3.61946	3.24167
2009-08	1.93854	2.51522	3.47610	3.46209	3.10072
2009-09	1.95616	2.53808	3.50770	3.49356	3.12891
2009-10	1.92092	2.49236	3.44451	3.43063	3.07254
2010-01	1.92092	2.49236	3.44451	3.43063	3.07254
Burn up [% FIMA]	9.31	11.60	14.84	14.74	13.50

4 RESULTS FOR HFR-EU1/3 AND HFR-EU1/4

4.1 Calculation characteristics and reported results

All calculations were performed using VESTA 2.1.5 and the internal PHOENIX depletion module (no transport calculations are required because of the use of the unperturbed neutron spectra). The calculations are performed using the JEFF 3.1 [9] nuclear data library at 900 K. This includes the required cross section data for the transport and reaction rate calculation, but also the neutron induced fission yield data, radioactive decay data and energy dependent isomeric branching ratio data. Cross section data and isomeric branching ratio data for isotopes that are not in the employed nuclear data libraries are taken from an ORIGEN 2.2 base library (in this case PWRU50.LIB).

A total of three sets of results has been provided, one for the reference result after the normalisation of the irradiation history and an upper and lower burn up range calculation. The reference calculation contains the results for all spheres while the upper and lower burn up range calculations only contain results for HFR-EU1/3 and HFR-EU1/4 (which were normalised to the ^{137}Cs activity). In this chapter we will only highlight some of the results for the HFR-EU1/3 and HFR-EU1/4 spheres. This includes the final burn up values, a comparison with the measured activity values, the composition of specific nuclides of interest for HTR fuel behaviour and the power production during irradiation.

These three sets of results are provided on a separate DVD, along with a version of the AURORA tool to allow for further post-processing.

4.2 Burn up values

The scaling factors resulting from the normalisation on the ^{137}Cs activity and the upper and lower estimate for the burn up range for the HFR-EU1/3 and HFR-EU1/4 are given in Table 4.1. As mentioned earlier, the calculated reference burn up values are slightly higher than the reported values (14.84 % versus 13.90 % for HFR-EU1/3 and 14.74 % versus 14.30 % for HFR-EU1/4) but they are well within the uncertainty due to the normalisation. The upper and lower burn up estimates were made using the three sigma error on the ^{137}Cs activity measurements which translates to a three sigma error on the burn up value of roughly 1.3 % FIMA (i.e. a relative error of about 9 %).

Table 4.1 also gives the final burn up values in MWd kgHM^{-1}. Compared to a standard PWR reactor, these burn up values are exceptionally high, being 141.8 MWd kgHM^{-1} for HFR-EU1/3 and 140.9 MWd kgHM^{-1} for HFR-EU1/4. The high initial ^{235}U enrichment (which is about 4 times higher than what one would expect in a standard PWR reactor) makes these levels of burn up possible.

Table 4.1: Calculated burn up levels for the HFR-EU1/3 and HFR-EU1/4 spheres.

Sphere	HFR-EU1/3			HFR-EU1/4		
	Normalisation factor	Burn up [MWd kgHM^{-1}]	Burn up [% FIMA]	Normalisation factor	Burn up [MWd kgHM^{-1}]	Burn up [% FIMA]
Reference	0.72218	141.8	14.84	0.73166	140.9	14.74
Upper	0.80625	154.4	16.14	0.81615	153.3	16.02
Lower	0.64188	129.2	13.53	0.65072	128.4	13.45

4.3 Comparison with activity measurements

A number of activity measurements have been performed on the HFR-EU1/3 and HFR-EU1/4 spheres in the framework of the ARCHER project [19]. Two independent measurements were performed for the HFR-EU1/3 sphere (one measurement made on Febuary 3, 2014 and another measurement made on March 12, 2013) and only one for the HFR-EU1/4 sphere (on February 12, 2014). The activities were measured for ^{106}Ru, ^{110m}Ag, ^{125}Sb, ^{134}Cs, ^{137}Cs, ^{144}Ce, ^{154}Eu, ^{155}Eu and ^{241}Am and are reported at the end of irradiation. The C/E values for the reference burn up calculations and the upper and lower limit of the burn up range for these activity measurements are given in Table 4.2. The error values given correspond to one standard deviation.

Table 4.2: Comparison between calculated and measured activities of HFR-EU1/3 and HFR-EU1/4 for a single TRISO particle at the end of the irradiation.

Nuclide	HFR-EU1/3 measurement 1 (Febuary 3, 2014)			
	Measured activity [Bq]	Reference C/E	Lower C/E	Upper C/E
^{106}Ru	2.877E+7 ± 6.0 %	1.177 ± 0.071	1.015 ± 0.061	1.346 ± 0.081
^{110m}Ag	1.496E+5 ± 11.0 %	1.453 ± 0.161	1.102 ± 0.122	1.872 ± 0.207
^{125}Sb	4.749E+5 ± 6.7 %	1.439 ± 0.096	1.249 ± 0.083	1.641 ± 0.109
^{134}Cs	1.308E+7 ± 3.5 %	0.753 ± 0.026	0.617 ± 0.022	0.903 ± 0.032
^{137}Cs	9.969E+6 ± 2.9 %	0.998 ± 0.029	0.911 ± 0.026	1.084 ± 0.031
^{144}Ce	7.646E+7 ± 11.1 %	1.106 ± 0.123	1.038 ± 0.115	1.169 ± 0.130
^{154}Eu	3.808E+5 ± 7.5 %	0.955 ± 0.071	0.796 ± 0.059	1.123 ± 0.084
^{155}Eu	2.762E+5 ± 8.9 %	1.051 ± 0.094	0.894 ± 0.080	1.217 ± 0.108
^{241}Am	5.575E+4 ± 41.3 %	0.282 ± 0.117	0.259 ± 0.107	0.299 ± 0.124
Nuclide	HFR-EU1/3 measurement 2 (March 12, 2013)			
	Measured activity [Bq]	Reference C/E	Lower C/E	Upper C/E
^{106}Ru	2.866E+7 ± 11.1 %	1.181 ± 0.131	1.019 ± 0.113	1.351 ± 0.150
^{110m}Ag	1.475E+5 ± 16.0 %	1.474 ± 0.235	1.117 ± 0.178	1.898 ± 0.303
^{125}Sb	4.707E+5 ± 8.4 %	1.452 ± 0.122	1.260 ± 0.106	1.655 ± 0.139
^{134}Cs	1.266E+7 ± 4.5 %	0.778 ± 0.035	0.637 ± 0.029	0.932 ± 0.042
^{137}Cs	9.916E+6 ± 2.9 %	1.003 ± 0.030	0.916 ± 0.027	1.090 ± 0.032
^{144}Ce	7.542E+7 ± 24.5 %	1.121 ± 0.275	1.052 ± 0.258	1.185 ± 0.291
^{154}Eu	3.787E+5 ± 8.0 %	0.960 ± 0.077	0.800 ± 0.064	1.130 ± 0.091
^{155}Eu	2.897E+5 ± 9.5 %	1.002 ± 0.095	0.852 ± 0.081	1.160 ± 0.110
^{241}Am	5.000E+4 ± 46.0 %	0.315 ± 0.145	0.288 ± 0.133	0.334 ± 0.154
Nuclide	HFR-EU1/4 measurement (Febuary 12, 2014)			
	Measured activity [Bq]	Reference C/E	Lower C/E	Upper C/E
^{106}Ru	2.887E+7 ± 6.1 %	1.153 ± 0.070	0.996 ± 0.060	1.318 ± 0.080
^{110m}Ag	1.172E+5 ± 12.3 %	1.814 ± 0.224	1.377 ± 0.170	2.333 ± 0.287
^{125}Sb	4.644E+5 ± 6.7 %	1.452 ± 0.097	1.261 ± 0.084	1.654 ± 0.110
^{134}Cs	1.318E+7 ± 3.5 %	0.739 ± 0.026	0.607 ± 0.021	0.885 ± 0.031
^{137}Cs	9.874E+6 ± 2.9 %	1.001 ± 0.029	0.914 ± 0.026	1.086 ± 0.031
^{144}Ce	7.657E+7 ± 11.1 %	1.097 ± 0.122	1.030 ± 0.114	1.159 ± 0.128
^{154}Eu	3.828E+5 ± 7.5 %	0.938 ± 0.070	0.782 ± 0.059	1.102 ± 0.082
^{155}Eu	2.803E+5 ± 8.8 %	1.025 ± 0.091	0.873 ± 0.077	1.187 ± 0.105
^{241}Am	5.031E+4 ± 41.4 %	0.310 ± 0.128	0.283 ± 0.117	0.329 ± 0.136

It is possible to incorporate both the uncertainty for a single nuclide due to the experimental measurements and the uncertainty due to the irradiation history normalisation into a single graph of C/E as a function of burn up using a non regular hexagon, as illustrated in Figure 4.1 and 4.2. The six points of the hexagon are defined as $(C/E)_l \pm 3\sigma_l$ (lower value of the burn up range), $(C/E)_r \pm 3\sigma_r$ (reference burn up) and $(C/E)_u \pm 3\sigma_u$ (upper value of the burn up range). The "midpoint" of the hexagon is the reference C/E value at the reference burn up. The depicted uncertainty range corresponds with a three sigma uncertainty.

This type of representation works very well for communicating the sensitivity to the burn up level of the sample for a given nuclide. The form of the hexagon gives for instance an indication if the dependence on burn up is linear or exponential. The "slope" of the hexagon on the other hand is a measure of the derivative of the C/E value to burn up and thus an indication on how sensitive a particular nuclide is to the burn up itself.

Figure 4.1 gives these hexagons for the first 6 nuclides (^{106}Ru, ^{110m}Ag, ^{125}Sb, ^{134}Cs, ^{137}Cs and ^{144}Ce) while Figure 4.2 gives the hexagons for the remaining 3 nuclides (^{154}Eu, ^{155}Eu and ^{241}Am).

All nuclides exhibit a positive sensitivity with respect to burn up, which is to be excepted because these nuclides are all fission products (with the exception of ^{241}Am). The highest sensitivities are observed for ^{110m}Ag. The form of the uncertainty area for this nuclide indicates that the sensitivity is not completely linear but more likely exponential. An increase of the burn up by about 10 % changes the C/E value for the HFR-EU1/3 sphere from ± 1.45 to about ± 1.9 (a 31 % change). The lowest sensitivity is observed for ^{144}Ce and ^{241}Am. In these cases, the C/E value as a function of burn up is almost constant: an increase of the burn up by 10 % increases the C/E value from ± 1.10 to ± 1.17 (a 6 % change) for ^{144}Ce and from ± 0.3 to ± 0.33 (a 10 % change) for ^{241}Am.

In view of the various approximations made for the modelling (for example the use of only three representative spectra for the entire irradiation) and the reported measurement errors, the calculated to experimental values are quite good. A first observation that we can make is that the measurements for the HFR-EU1/3 and HFR-EU1/4 spheres are always quite close. In view of the small difference in burn up, this is to be expected. The only exception is ^{110m}Ag where the result for HFR-EU1/4 is higher than the results for HFR-EU1/3, although the results are still within the three sigma uncertainty range.

With the exception of ^{125}Sb, ^{134}Cs and ^{241}Am for all measurements and ^{110m}Ag for HFR-EU1/4, the obtained C/E values are always well within the three sigma uncertainty range. The ^{137}Cs values are spot on because the irradiation history was normalised on these measurements. The results for the Eu measurements are nicely within one sigma while the ^{106}Ru results are roughly within two sigma.

The overestimation of the ^{125}Sb activity by 50 % is most likely a cross section problem, and not the result of other experimental issues. A review of relevant cross section data showed that there exist two different evaluations in the case of ^{125}Sb. The first being an old ENDF/B-V evaluation which is used in JEF 2.2, JEFF 3.0, JEFF 3.1 and ENDF/B-VI.8 and a second more recent evaluation prepared for JENDL 3 which will be adopted in ENDF/B-VII. The neutron capture cross sections for these two different evaluations are shown in figure 4.3. The difference between both evaluations in the $1/v$ component of this cross section is a factor 5 while the cross section values above 100 eV are rather similar for both evaluations. The cross section jump at 10 eV for the JENDL evaluation and 100 eV for the JEFF 3.1 evaluation also indicates a more fundamental problem, namely the lack of experimental cross section and resonance data with which a proper

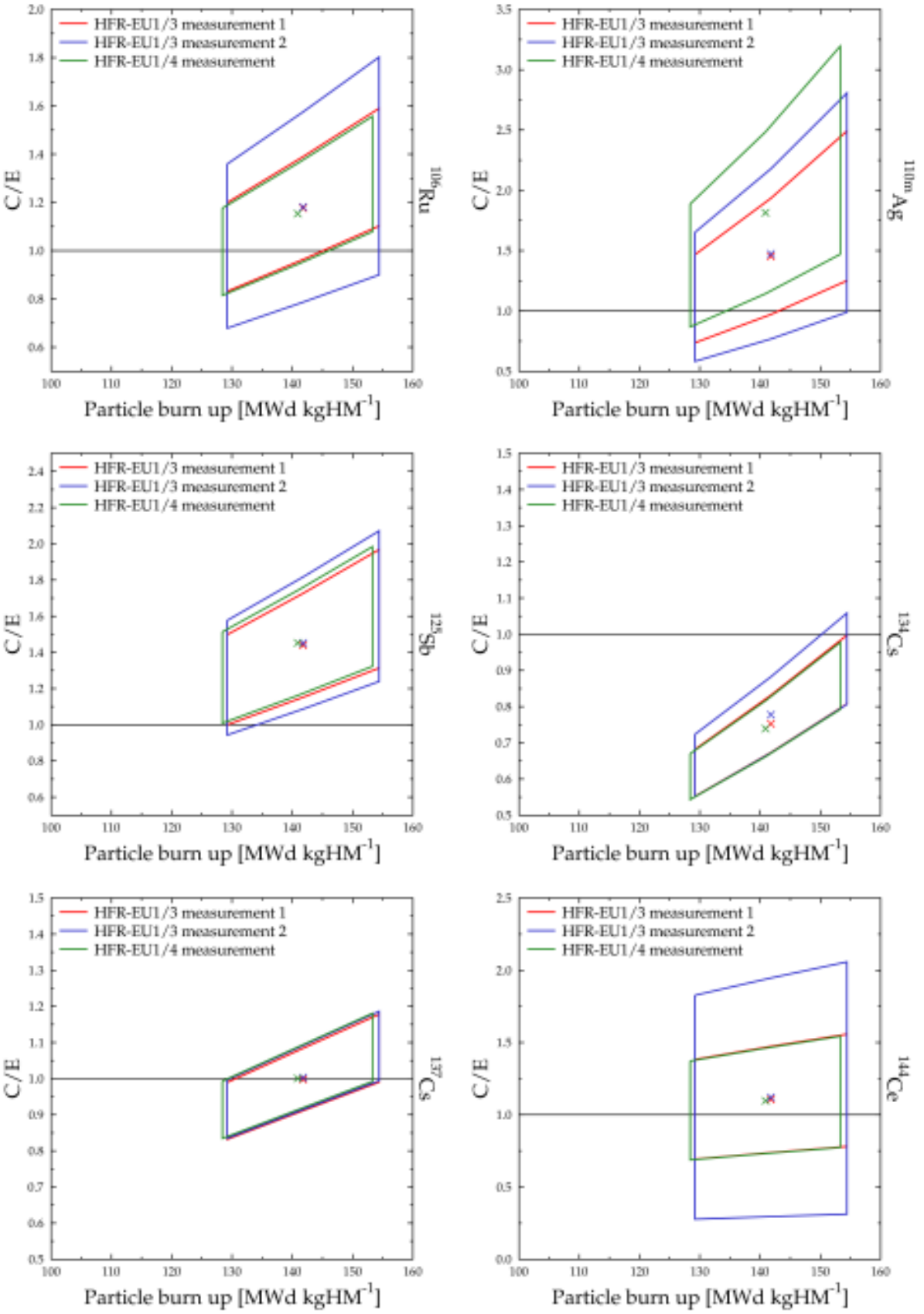

Figure 4.1: Comparison between calculated and measured activities of ^{106}Ru, ^{110m}Ag, ^{125}Sb, ^{134}Cs, ^{137}Cs and ^{144}Ce of HFR-EU1/3 and HFR-EU1/4 for a single TRISO particle at the end of the irradiation.

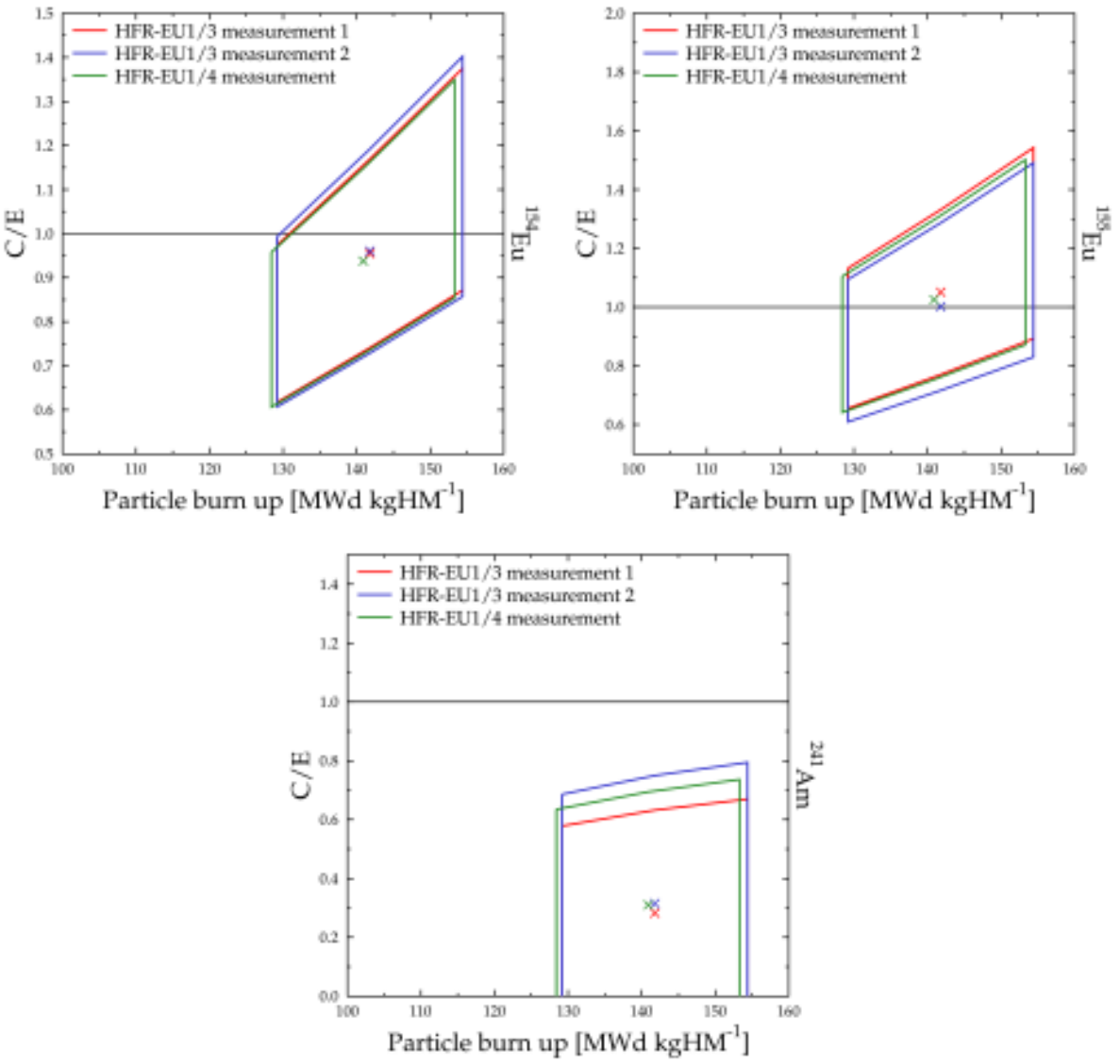

Figure 4.2: Comparison between calculated and measured activities of ^{154}Eu, ^{155}Eu and ^{241}Am of HFR-EU1/3 and HFR-EU1/4 for a single TRISO particle at the end of the irradiation.

cross section can be constructed.

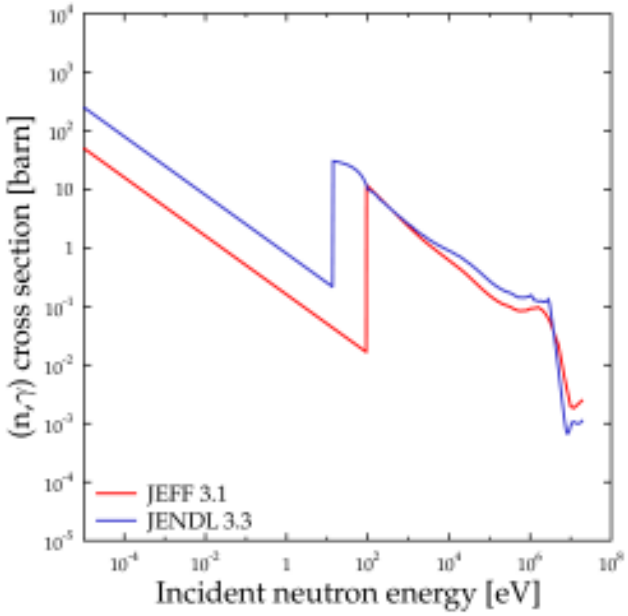

Figure 4.3: The ^{125}Sb neutron capture cross section from the JEFF 3.1 and JENDL 3.3 nuclear data libraries.

4.4 Nuclide compositions

4.4.1 Actinides

Table 4.3 and Table 4.4 give the final compositions for the HFR-EU1/3 and HFR-EU1/4 spheres, averaged to a single TRISO particle. The compositions are given both in μg and in 10^{24} atoms. As for the previous comparison with the activity measurements, the results are given for the reference calculation and for the upper and lower burn up range. The final burn up levels of each sphere are quite close, which is reflected in these compositions (the results are very close).

Each TRISO particle has about 104.6 μg of ^{235}U (a single AVR sphere contains 1 g of ^{235}U) and 519.5 μg of ^{238}U. Of that initial amount, about 28 μg of ^{235}U (26.8 % of the initial amount) and 473 μg of ^{238}U (91 % of the initial amount) remain. The main transmutation path for ^{238}U is the production of ^{239}Pu. At the end of irradiation, about 12 μg of ^{239}Pu is present in the particle, which means that over the course of the irradiation we will have consumed about 34.5 μg of ^{239}Pu through fission and further transmutation into other Pu, Am and Cm isotopes. At the end of the irradiation, we thus have about 20 μg of Pu, 0.24 μg of Am and 81.3 ng of Cm in the average TRISO particle.

As with the activity measurements, the results for the lower and upper burn up range allow us to assess the sensitivity of each individual nuclide as a function of burn up. Contrary to what we observed for the activity measurements (where we only saw positive sensitivities), we now have nuclides with a positive or negative sensitivity which indicate an average production or consumption at this burn up level. ^{235}U and ^{238}U are the only nuclides with a negative sensitivity. All other nuclides with the exception of ^{239}Pu and ^{242m}Am have a positive sensitivity to burn up. The cases of ^{239}Pu and ^{242m}Am are a bit peculiar.

Table 4.3: U, Np, Pu, Am and Cm content in HFR-EU1/3 for a single TRISO particle at the end of the irradiation.

Nuclide	Composition [10^{24} atoms]			
	Initial	Reference	Lower	Upper
^{234}U	-	6.255E-12	5.413E-12	7.195E-12
^{235}U	2.680E-7	7.198E-8	8.330E-8	6.176E-8
^{236}U	-	3.058E-8	2.910E-8	3.184E-8
^{238}U	1.314E-6	1.195E-6	1.208E-6	1.182E-6
^{237}Np	-	1.840E-9	1.564E-9	2.126E-9
^{239}Np	-	9.417E-10	8.461E-10	1.040E-9
^{238}Pu	-	4.012E-10	3.072E-10	5.095E-10
^{239}Pu	-	2.999E-8	2.991E-8	2.992E-8
^{240}Pu	-	1.003E-8	9.572E-9	1.035E-8
^{241}Pu	-	7.869E-9	7.013E-9	8.605E-9
^{242}Pu	-	2.821E-9	2.149E-9	3.578E-9
^{241}Am	-	3.103E-10	2.840E-10	3.287E-10
^{242m}Am	-	5.969E-12	5.394E-12	6.382E-12
^{243}Am	-	2.825E-10	1.888E-10	4.049E-10
^{242}Cm	-	1.548E-10	1.215E-10	1.899E-10
^{243}Cm	-	1.539E-12	1.080E-12	2.094E-12
^{244}Cm	-	4.444E-11	2.582E-11	7.272E-11
^{245}Cm	-	1.049E-12	5.583E-13	1.856E-12
^{246}Cm	-	8.763E-14	4.059E-14	1.770E-13
Nuclide	Composition [μg]			
	Initial	Reference	Lower	Upper
^{234}U	-	2.431E-3	2.104E-3	2.796E-3
^{235}U	1.046E+2	2.809E+1	3.251E+1	2.411E+1
^{236}U	-	1.199E+1	1.141E+1	1.248E+1
^{238}U	5.195E+2	4.726E+2	4.776E+2	4.674E+2
^{237}Np	-	7.243E-1	6.156E-1	8.370E-1
^{239}Np	-	3.738E-1	3.359E-1	4.127E-1
^{238}Pu	-	1.586E-1	1.214E-1	2.014E-1
^{239}Pu	-	1.191E+1	1.187E+1	1.188E+1
^{240}Pu	-	3.996E+0	3.816E+0	4.126E+0
^{241}Pu	-	3.150E+0	2.807E+0	3.444E+0
^{242}Pu	-	1.134E+0	8.637E-1	1.438E+0
^{241}Am	-	1.242E-1	1.137E-1	1.316E-1
^{242m}Am	-	2.399E-3	2.168E-3	8.078E-4
^{243}Am	-	1.140E-1	7.622E-2	1.634E-1
^{242}Cm	-	6.221E-2	4.885E-2	7.634E-2
^{243}Cm	-	6.210E-4	4.359E-4	8.453E-4
^{244}Cm	-	1.801E-2	1.047E-2	2.947E-2
^{245}Cm	-	4.267E-4	2.272E-4	7.552E-4
^{246}Cm	-	3.581E-5	1.658E-5	7.233E-5

Table 4.4: U, Np, Pu, Am and Cm content in HFR-EU1/4 for a single TRISO particle at the end of the irradiation.

Nuclide	Composition [10^{24} atoms]			
	Initial	Reference	Lower	Upper
^{234}U	-	6.195E-12	5.369E-12	7.115E-12
^{235}U	2.680E-7	7.247E-8	8.375E-8	6.231E-8
^{236}U	-	3.054E-8	2.906E-8	3.180E-8
^{238}U	1.314E-6	1.197E-6	1.210E-6	1.184E-6
^{237}Np	-	1.821E-9	1.549E-9	2.103E-9
^{239}Np	-	9.232E-10	8.298E-10	1.018E-9
^{238}Pu	-	3.937E-10	3.017E-10	4.993E-10
^{239}Pu	-	2.962E-8	2.954E-8	2.956E-8
^{240}Pu	-	9.939E-9	9.486E-9	1.026E-8
^{241}Pu	-	7.738E-9	6.895E-9	8.463E-9
^{242}Pu	-	2.757E-9	2.102E-9	3.494E-9
^{241}Am	-	3.071E-10	2.808E-10	3.257E-10
^{242m}Am	-	5.883E-12	5.311E-12	6.297E-12
^{243}Am	-	2.771E-10	1.855E-10	3.965E-10
^{242}Cm	-	1.515E-10	1.190E-10	1.859E-10
^{243}Cm	-	1.480E-12	1.039E-12	2.012E-12
^{244}Cm	-	4.317E-11	2.514E-11	7.043E-11
^{245}Cm	-	1.021E-12	5.452E-13	1.802E-12
^{246}Cm	-	8.497E-14	3.948E-14	1.709E-13
Nuclide	Composition [μg]			
	Initial	Reference	Lower	Upper
^{234}U	-	2.408E-3	2.086E-3	2.765E-3
^{235}U	1.046E+2	2.829E+1	3.269E+1	2.432E+1
^{236}U	-	1.197E+1	1.139E+1	1.246E+1
^{238}U	5.195E+2	4.733E+2	4.782E+2	4.682E+2
^{237}Np	-	7.169E-1	6.096E-1	8.279E-1
^{239}Np	-	3.665E-1	3.294E-1	4.043E-1
^{238}Pu	-	1.556E-1	1.193E-1	1.974E-1
^{239}Pu	-	1.176E+1	1.173E+1	1.173E+1
^{240}Pu	-	3.962E+0	3.781E+0	4.091E+0
^{241}Pu	-	3.097E+0	2.760E+0	3.388E+0
^{242}Pu	-	1.108E+0	8.448E-1	1.404E+0
^{241}Am	-	1.229E-1	1.124E-1	1.304E-1
^{242m}Am	-	2.365E-3	2.135E-3	7.929E-4
^{243}Am	-	1.118E-1	7.485E-2	1.600E-1
^{242}Cm	-	6.091E-2	4.785E-2	7.472E-2
^{243}Cm	-	5.972E-4	4.195E-4	8.121E-4
^{244}Cm	-	1.749E-2	1.019E-2	2.855E-2
^{245}Cm	-	4.157E-4	2.219E-4	7.333E-4
^{246}Cm	-	3.472E-5	1.613E-5	6.983E-5

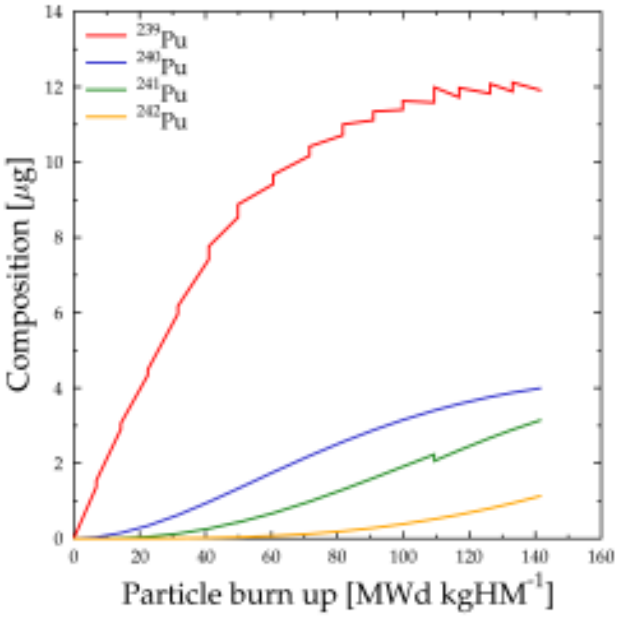

Figure 4.4: Pu content in the HFR-EU1/3 sphere averaged to a single TRISO particle as a function of burn up.

^{239}Pu has an almost constant sensitivity (the ratio of the ^{239}Pu composition at the upper and lower burn up range to the reference value is 0.997 in both cases) which indicates a competition between ^{239}Pu production and consumption. This is illustrated in Figure 4.4 which gives the Pu content of the average TRISO particle for HFR-EU1/3 as a function of burn up.

The small 'jumps' in the ^{239}Pu curve represent the shutdown periods in between the HFR reactor cycles. The ^{239}Pu content increases over these shutdown periods due to the decay of ^{239}Np. Each segment in between those 'jumps' therefore corresponds with an HFR reactor cycle. These jumps are only visible for ^{239}Pu. ^{241}Pu exhibits a single jump, which corresponds to the shutdown period of 603.24 days between cycles 2008-02 and 2009-08. During this shutdown period, a significant amount of ^{241}Pu decayed to ^{241}Am.

The ^{239}Pu increases almost linearly at the beginning of the irradiation for the first 6 reactor cycles (up to 40 MWd kgHM^{-1}) after which the accumulation of ^{239}Pu slows down. Up until the 12th irradiation cycle (HFR cycle 2008-02), we observe a net ^{239}Pu production over the cycle. After this cycle, we start to burn ^{239}Pu instead of producing it. The loss in ^{239}Pu is however compensated through ^{239}Np decay during the shutdown periods.

The level of sensitivity to the burn up also varies from nuclide to nuclide. ^{246}Cm has for instance the highest positive sensitivity for all nuclides in Tables 4.3 and 4.4. An increase in burn up of 10 % (which corresponds to the upper burn up range) almost doubles the amount of ^{246}Cm. Inversely, a decrease of 10 % in burn up will halve the ^{246}Cm composition. The slightest error on burn up will thus have a significant impact on the Cm results.

4.4.2 Fission products

In the context of new hypotheses on the transport of Ag through perfect SiC in LEU TRISO particles, it is important to know the inventories of Pd, Ag and Cd in the particles. Tables 4.5 up

to 4.7 give these data for the end of the irradiation for HFR-EU1/3 and HFR-EU1/4 for each important isotope of Pd, Ag and Cd. As before, the reference result is given along with the upper and lower estimate of the burn up range.

Figure 4.5 gives the evolution of the total Pd, Ag and Cd content for the average TRISO particle of HFR-EU1/3. As with the Pu content in Figure 4.4, the small 'jumps' in the Pd, Ag and Cd curves represent the shutdown periods in between the HFR reactor cycles.

Table 4.8 gives the final compositions for some fission products for the HFR-EU1/3 and HFR-EU1/4 spheres, averaged to a single TRISO particle. The compositions are given both in μg and in 10^{24} atoms. The selected fission products are important for fission gas release.

Table 4.5: Pd content in HFR-EU1/3 (left) and HFR-EU1/4 (right) for a single TRISO particle at the end of the irradiation.

Nuclide	HFR-EU1/3 Composition [10^{24} atoms]			HFR-EU1/4 Composition [10^{24} atoms]		
	Reference	Lower	Upper	Reference	Lower	Upper
^{102}Pd	4.222E-16	3.398E-16	5.156E-16	4.096E-16	3.300E-16	4.996E-16
^{103}Pd	2.606E-16	1.873E-16	3.536E-16	2.513E-16	1.809E-16	3.403E-16
^{104}Pd	2.090E-9	1.692E-9	2.536E-9	2.059E-9	1.670E-9	2.496E-9
^{105}Pd	4.756E-9	4.196E-9	5.329E-9	4.699E-9	4.149E-9	5.261E-9
^{106}Pd	2.702E-9	2.259E-9	3.193E-9	2.667E-9	2.232E-9	3.148E-9
^{107}Pd	2.487E-9	2.105E-9	2.897E-9	2.449E-9	2.075E-9	2.850E-9
^{108}Pd	1.636E-9	1.372E-9	1.923E-9	1.610E-9	1.351E-9	1.890E-9
^{109}Pd	3.999E-12	3.400E-12	4.629E-12	3.918E-12	3.333E-12	4.531E-12
^{110}Pd	5.721E-10	4.753E-10	6.782E-10	5.627E-10	4.679E-10	6.663E-10
^{111}Pd	2.000E-14	1.727E-14	2.280E-14	1.961E-14	1.694E-14	2.234E-14
^{111m}Pd	1.720E-15	1.477E-15	1.976E-15	1.686E-15	1.449E-15	1.936E-15
^{112}Pd	4.299E-13	3.736E-13	4.876E-13	4.218E-13	3.669E-13	4.780E-13
Pd	1.425E-8	1.210E-8	1.656E-8	1.405E-8	1.195E-8	1.632E-8
Nuclide	HFR-EU1/3 Composition [μg]			HFR-EU1/4 Composition [μg]		
	Reference	Lower	Upper	Reference	Lower	Upper
^{102}Pd	7.144E-8	5.750E-8	8.725E-8	6.932E-8	5.585E-8	8.454E-8
^{103}Pd	4.453E-8	3.201E-8	6.042E-8	4.295E-8	3.092E-8	5.815E-8
^{104}Pd	3.606E-1	2.920E-1	4.375E-1	3.553E-1	2.881E-1	4.306E-1
^{105}Pd	8.285E-1	7.309E-1	9.283E-1	8.186E-1	7.228E-1	9.165E-1
^{106}Pd	4.752E-1	3.972E-1	5.616E-1	4.691E-1	3.926E-1	5.536E-1
^{107}Pd	4.415E-1	3.737E-1	5.143E-1	4.348E-1	3.684E-1	5.059E-1
^{108}Pd	2.932E-1	2.458E-1	3.446E-1	2.885E-1	2.420E-1	3.386E-1
^{109}Pd	7.232E-4	6.148E-4	8.371E-4	7.085E-4	6.028E-4	8.194E-4
^{110}Pd	1.044E-1	8.674E-2	1.238E-1	1.027E-1	8.540E-2	1.216E-1
^{111}Pd	3.683E-6	3.180E-6	4.200E-6	3.611E-6	3.120E-6	4.115E-6
^{111m}Pd	3.168E-7	2.721E-7	3.639E-7	3.106E-7	2.669E-7	3.565E-7
^{112}Pd	7.989E-5	6.943E-5	9.062E-5	7.839E-5	6.817E-5	8.883E-5
Pd	2.504E+0	2.127E+0	2.911E+0	2.470E+0	2.100E+0	2.868E+0

Table 4.6: Ag content in HFR-EU1/3 (left) and HFR-EU1/4 (right) for a single TRISO particle at the end of the irradiation.

Nuclide	HFR-EU1/3 Composition [10^{24} atoms]			HFR-EU1/4 Composition [10^{24} atoms]		
	Reference	Lower	Upper	Reference	Lower	Upper
^{107}Ag	4.087E-16	3.448E-16	4.781E-16	4.036E-16	3.407E-16	4.715E-16
^{108m}Ag	8.856E-17	7.580E-17	1.020E-16	8.720E-17	7.468E-17	1.003E-16
^{109}Ag	1.026E-9	8.799E-10	1.178E-9	1.011E-9	8.671E-10	1.159E-9
^{109m}Ag	3.209E-15	2.728E-15	3.714E-15	3.144E-15	2.675E-15	3.636E-15
^{110}Ag	6.437E-16	4.905E-16	8.247E-16	6.287E-16	4.797E-16	8.042E-16
^{110m}Ag	6.767E-12	5.131E-12	8.716E-12	6.618E-12	5.024E-12	8.510E-12
^{111}Ag	9.001E-12	7.755E-12	1.029E-11	8.826E-12	7.610E-12	1.008E-11
^{111m}Ag	9.191E-16	7.933E-16	1.049E-15	9.012E-16	7.784E-16	1.027E-15
^{112}Ag	6.648E-14	5.776E-14	7.543E-14	6.522E-14	5.671E-14	7.394E-14
^{113}Ag	5.146E-14	4.522E-14	5.784E-14	5.056E-14	4.446E-14	5.677E-14
Ag	1.042E-9	8.929E-10	1.197E-9	1.026E-9	8.799E-10	1.178E-9
Nuclide	HFR-EU1/3 Composition [μg]			HFR-EU1/4 Composition [μg]		
	Reference	Lower	Upper	Reference	Lower	Upper
^{107}Ag	7.256E-8	6.120E-8	8.488E-8	7.164E-8	6.049E-8	8.371E-8
^{108m}Ag	1.587E-8	1.358E-8	1.827E-8	1.562E-8	1.338E-8	1.798E-8
^{109}Ag	1.856E-1	1.591E-1	2.130E-1	1.828E-1	1.568E-1	2.096E-1
^{109m}Ag	5.803E-7	4.934E-7	6.717E-7	5.686E-7	4.837E-7	6.575E-7
^{110}Ag	1.175E-7	8.952E-8	1.505E-7	1.147E-7	8.755E-8	1.468E-7
^{110m}Ag	1.235E-3	9.364E-4	1.591E-3	1.208E-3	9.170E-4	1.553E-3
^{111}Ag	1.658E-3	1.428E-3	1.895E-3	1.625E-3	1.401E-3	1.856E-3
^{111m}Ag	1.693E-7	1.461E-7	1.931E-7	1.660E-7	1.434E-7	1.892E-7
^{112}Ag	1.235E-5	1.073E-5	1.402E-5	1.212E-5	1.054E-5	1.374E-5
^{113}Ag	9.649E-6	8.477E-6	1.084E-5	9.480E-6	8.336E-6	1.064E-5
Ag	1.885E-1	1.615E-1	2.165E-1	1.856E-1	1.592E-1	2.130E-1

Table 4.7: Cd content in HFR-EU1/3 (left) and HFR-EU1/4 (right) for a single TRISO particle at the end of the irradiation.

Nuclide	HFR-EU1/3 Composition [10^{24} atoms]			HFR-EU1/4 Composition [10^{24} atoms]		
	Reference	Lower	Upper	Reference	Lower	Upper
^{108}Cd	1.921E-15	1.446E-15	2.494E-15	1.839E-15	1.387E-15	2.384E-15
^{109}Cd	6.846E-17	4.597E-17	9.887E-17	6.543E-17	4.403E-17	9.424E-17
^{110}Cd	2.655E-10	1.995E-10	3.452E-10	2.599E-10	1.956E-10	3.374E-10
^{111}Cd	2.401E-10	2.038E-10	2.792E-10	2.365E-10	2.010E-10	2.747E-10
^{112}Cd	1.151E-10	9.787E-11	1.337E-10	1.134E-10	9.656E-11	1.317E-10
^{113}Cd	1.240E-12	1.223E-12	1.250E-12	1.226E-12	1.210E-12	1.236E-12
^{113m}Cd	1.013E-12	8.640E-13	1.175E-12	9.994E-13	8.537E-13	1.158E-12
^{114}Cd	1.449E-10	1.256E-10	1.655E-10	1.432E-10	1.242E-10	1.632E-10
^{115}Cd	4.673E-13	4.052E-13	5.314E-13	4.592E-13	3.986E-13	5.216E-13
^{115m}Cd	3.421E-13	2.954E-13	3.910E-13	3.364E-13	2.908E-13	3.840E-13
^{116}Cd	6.116E-11	5.374E-11	6.897E-11	6.051E-11	5.321E-11	6.815E-11
Cd	8.298E-10	6.833E-10	9.959E-10	8.166E-10	6.734E-10	9.785E-10
Nuclide	HFR-EU1/3 Composition [μg]			HFR-EU1/4 Composition [μg]		
	Reference	Lower	Upper	Reference	Lower	Upper
^{108}Cd	3.441E-7	2.591E-7	4.469E-7	3.296E-7	2.485E-7	4.272E-7
^{109}Cd	1.238E-8	8.314E-9	1.788E-8	1.183E-8	7.962E-9	1.704E-8
^{110}Cd	4.845E-2	3.641E-2	6.300E-2	4.744E-2	3.570E-2	6.158E-2
^{111}Cd	4.421E-2	3.753E-2	5.141E-2	4.356E-2	3.701E-2	5.060E-2
^{112}Cd	2.139E-2	1.819E-2	2.485E-2	2.108E-2	1.794E-2	2.447E-2
^{113}Cd	2.324E-4	2.294E-4	2.343E-4	2.298E-4	2.269E-4	2.317E-4
^{113m}Cd	1.898E-4	1.620E-4	2.203E-4	1.874E-4	1.601E-4	2.172E-4
^{114}Cd	2.741E-2	2.376E-2	3.131E-2	2.708E-2	2.350E-2	3.087E-2
^{115}Cd	8.916E-5	7.732E-5	1.014E-4	8.762E-5	7.605E-5	9.953E-5
^{115m}Cd	6.528E-5	5.637E-5	7.460E-5	6.419E-5	5.548E-5	7.327E-5
^{116}Cd	1.177E-2	1.034E-2	1.327E-2	1.165E-2	1.024E-2	1.312E-2
Cd	1.538E-1	1.268E-1	1.845E-1	1.514E-1	1.249E-1	1.812E-1

Table 4.8: Fission product content in HFR-EU1/3 (left) and HFR-EU1/4 (right) for a single TRISO particle at the end of the irradiation.

Nuclide	HFR-EU1/3 Composition [10^{24} atoms]			HFR-EU1/4 Composition [10^{24} atoms]		
	Reference	Lower	Upper	Reference	Lower	Upper
^{85}Kr	4.816E-10	4.474E-10	5.143E-10	4.794E-10	4.454E-10	5.116E-10
^{85m}Kr	1.024E-12	9.992E-13	1.041E-12	1.019E-12	9.941E-13	1.035E-12
^{89}Sr	7.768E-10	7.568E-10	7.899E-10	7.735E-10	7.537E-10	7.864E-10
^{90}Sr	1.009E-8	9.395E-9	1.074E-8	1.005E-8	9.359E-9	1.069E-8
^{106}Ru	1.572E-9	1.356E-9	1.799E-9	1.546E-9	1.335E-9	1.767E-9
^{131}I	1.592E-10	1.483E-10	1.695E-10	1.574E-10	1.468E-10	1.675E-10
^{133}I	3.604E-11	3.383E-11	3.810E-11	3.567E-11	3.351E-11	3.768E-11
^{133}Xe	2.099E-10	1.968E-10	2.221E-10	2.077E-10	1.950E-10	2.196E-10
^{135}Xe	1.957E-12	2.031E-12	1.881E-12	1.944E-12	2.019E-12	1.869E-12
^{134}Cs	9.252E-10	7.586E-10	1.109E-9	9.159E-10	7.517E-10	1.097E-9
^{137}Cs	1.360E-8	1.242E-8	1.478E-8	1.351E-8	1.234E-8	1.467E-8
Nuclide	HFR-EU1/3 Composition [μg]			HFR-EU1/4 Composition [μg]		
	Reference	Lower	Upper	Reference	Lower	Upper
^{85}Kr	6.791E-2	6.308E-2	7.252E-2	6.759E-2	6.281E-2	7.214E-2
^{85m}Kr	1.444E-4	1.409E-4	1.468E-4	1.436E-4	1.402E-4	1.460E-4
^{89}Sr	1.147E-1	1.117E-1	1.166E-1	1.142E-1	1.113E-1	1.161E-1
^{90}Sr	1.506E+0	1.403E+0	1.604E+0	1.500E+0	1.397E+0	1.596E+0
^{106}Ru	2.765E-1	2.385E-1	3.163E-1	2.719E-1	2.348E-1	3.107E-1
^{131}I	3.460E-2	3.223E-2	3.685E-2	3.422E-2	3.191E-2	3.641E-2
^{133}I	7.954E-3	7.466E-3	8.409E-3	7.873E-3	7.396E-3	8.316E-3
^{133}Xe	4.632E-2	4.344E-2	4.901E-2	4.585E-2	4.303E-2	4.847E-2
^{135}Xe	4.383E-4	4.550E-4	4.213E-4	4.356E-4	4.522E-4	4.187E-4
^{134}Cs	2.057E-1	1.687E-1	2.467E-1	2.037E-1	1.672E-1	2.439E-1
^{137}Cs	3.093E+0	2.823E+0	3.361E+0	3.072E+0	2.806E+0	3.336E+0

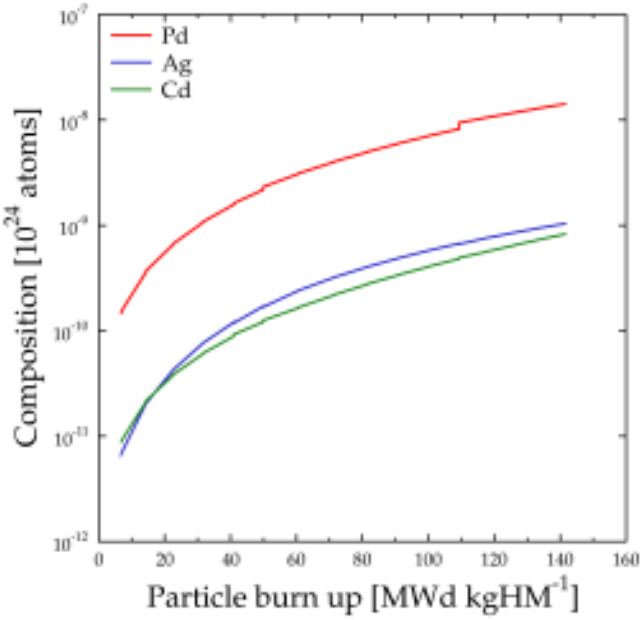

Figure 4.5: Pd, Ag and Cd content in the HFR-EU1/3 sphere averaged to a single TRISO particle as a function of burn up.

4.5 Power production

Figure 4.6 gives the total power produced in the HFR-EU1/3 and HFR-EU1/4 spheres averaged to a single TRISO particle as a function of burn up along with the power produced through fission of ^{235}U, ^{239}Pu and ^{241}Pu. The power values were used during the irradiation are given as constant power over a reactor cycle. The highest power value is of the order of 2.5 W averaged per TRISO particle (or 23.9 kW per sphere) and is achieved at the beginning of the third irradiation campaign.

The most important power producing actinides are ^{235}U, ^{239}Pu and ^{241}Pu which are responsible for 99.7 % of the total power in the beginning of the irradiation and 99.3 % of the total power at the end of the irradiation. The remainder is mainly due to fission of ^{238}U which is responsible for 0.3 % of the total power in the beginning and 0.6 % of the total power at the end of the irradiation.

Due to the high ^{235}U enrichment (of the order of 17 %), the majority of the power is produced by ^{235}U fission: 99.7 % at the beginning of the irradiation and still 47.7 % at the end of the irradiation (for a total burn up of about 140 MWd kgHM^{-1}). The importance of ^{239}Pu in the power production increases rapidly below 50 MWd kgHM^{-1} after which it slows down (this is due to a slow down in the net ^{239}Pu, see section 4.4.1). At the end of the irradiation, about 40 % of the total power is produced by ^{239}Pu.

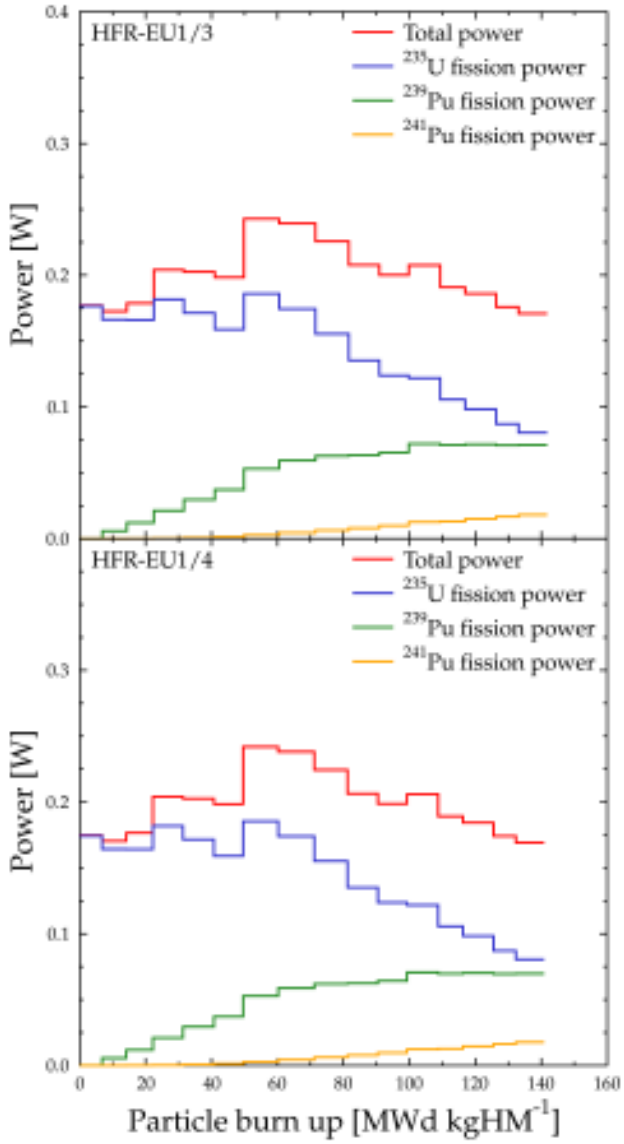

Figure 4.6: Power production in the HFR-EU1/3 and HFR-EU1/4 spheres averaged to a single TRISO particle: total power and fission power produced by ^{235}U, ^{239}Pu and ^{241}Pu.

5 CONCLUSIONS

This report presents the final conclusions of Task 3.2.3 (HFR-EU1 Irradiation modelling) of SP3 of the ARCHER project. The objective is to provide a source term of the TRISO particles in the fuel pebbles and accurate neutronics data for fuel performance calculations such as single group averaged cross sections as a function of time. To fullfill this objective, a new model that takes into account the variation as a function of burn up of the isomeric branching ratio for isomeric states (such as ^{242m}Am or ^{110m}Ag) has been implemented in the VESTA software. This has been applied to the HFR-EU1 irradiation experiment (in which several fuel pebbles were irradiated in the HFR in Petten).

The HFR fuel spheres have been modelled using unperturbed neutron spectra for each of the three reactor positions in which the irradiation rig was placed. Even though this approach represents an important approximation, it was deemed acceptable due to the limited amount of fissile material present in each sphere (which is less than 5 g for all fuel pebbles combined) so that the neutron spectrum that dominates the irradiation of the pebbles is the spectrum produced around the irradiation rig.

A number of activity measurements have been performed on the HFR-EU1/3 and HFR-EU1/4 spheres in the framework of the ARCHER project [19]. Two independent measurements were performed for the HFR-EU1/3 sphere (one measurement made on Febuary 3, 2014 and another measurement made on March 12, 2013) and only one for the HFR-EU1/4 sphere (on February 12, 2014). The activities were measured for ^{106}Ru, ^{110m}Ag, ^{125}Sb, ^{134}Cs, ^{137}Cs, ^{144}Ce, ^{154}Eu, ^{155}Eu and ^{241}Am and are reported at the end of irradiation. The comparison of our calculations with the experimental values is very satisfactory with the exception of the results for ^{241}Am.

The final burn up of the HFR fuel spheres at the end of the irradiation is quite high (of the order of 140 MWd kgHM^{-1}). Irradiated fuel at this level of burn up is rather scarce. As a result, a thorough radiochemical analysis should be envisaged. Such data can not only be used to study fission product release for this type of fuel but also be applied in a more general fashion in code validation (fuel performance codes and depletion codes). In addition, these additional experimental results can also be used to further verify the calculations presented in this report.

BIBLIOGRAPHY

[1] L. GOLYAND, E. SHWAGERAUS, Y. RONEN, "Effect of $^{241}_{95}$Am(n,γ) Reaction Branching Ratio on Fuel Cycle and Reactor Design Characteristics", *Nucl. Sci. Eng.*, **161**, pp 289-302 (2009)

[2] P. BOTAZZOLI, L. LUZZI, S. BREMIER, A. SCHUBERT, P. VAN UFFELEN, C. T. WALKER, W. HAECK, W. GOLL, "Extension and Validation of the TRANSURANUS Burn-up Model for Helium Production in High Burn-up LWR Fuels", Accepted for publication in *J. Nucl. Mat.* (2011)

[3] W. HAECK, "VESTA User's Manual - Version 2.1.0", IRSN DSU/SEC/T/2011-81 - Index A, Institut de Radioprotection et de Sûreté Nucléaire, France (2012)

[4] W. HAECK, B. COCHET, L. AGUIAR, "Burn-up dependent isomeric branching ratio treatment", *Nucl. Sci. Eng.*, **171**, pp 52-68 (2012)

[5] J. S. HENDRICKS, "MCNPX, VERSION 2.6.a", LA-UR-05-8225, Los Alamos National Laboratory, USA (2005)

[6] A. G. CROFF, "A User's Manual for the ORIGEN2 Computer Code", ORNL/TM-7175, Oak Ridge National Laboratory, USA (1980)

[7] R. Sanchez, I. Zmijarevic, M. Coste-Delclaux, E. Masiello, S. Santandrea, E. Martinolli, L. Villate, N. Schwartz, N. Guler, "APOLLO2 Year 2010", *Nucl. Eng. Tech.*, **42**, pp 474-499 (2010)

[8] M. B. CHADWICK et al., "ENDF/B-VII.0: Next Generation Evaluated Nuclear Data Library for Nuclear Science and Technology", *Nuclear Data Sheets*, **107**, pp. 2931-3060 (2006)

[9] A. KONING, R. FORREST, M. KELLETT, R. MILLS, H. HENRIKSSON, Y. RUGAMA, "The JEFF 3.1 Nuclear Data Library", JEF report 21, Nuclear Energy Agency - Organisation for Economic Cooperation and Development, France (2006)

[10] K. Shibata, O. Iwamoto, T. Nakagawa, N. Iwamoto, A. Ichihara, S. Kunieda, S. Chiba, K. Furutaka, N. Otuka, T. Ohsawa, T. Murata, H. Matsunobu, A. Zukeran, S. Kamada, J. Katakura, "JENDL-4.0: A New Library for Nuclear Science and Engineering", *J. Nucl. Sci. Technol.*, to be published

[11] P. TALOU, T. KAWANO, P. G. YOUNG, M. B. CHADWICK, R. E. MacFARLANE, "Improved Evaluations of Neutron-Induced Reactions on Americium Isotopes", *Nucl. Sci. Eng.*, **155**, pp 84-95 (2007)

[12] M. HERMAN, "ENDF-102 - ENDF-6 Data Formats and Procedures for the Evaluated Nuclear Data File ENDF-VII", BNL-NCS-44945-01/04-Rev., Brookhaven National Laboratory, USA (2005)

[13] R. E. MacFARLANE, D. W. MUIR, "The NJOY Nuclear Data Processing System Version 91", LA-12470-M, Los Alamos National Laboratory, USA (1994)

[14] W. HAECK, "An optimum approach to Monte Carlo burn-up", PhD thesis, Ghent University, Belgium (2007)

[15] W. HAECK, B. VERBOOMEN, "An Optimum Approach to Monte Carlo Burn-Up", *Nucl. Sci. Eng.*, **156**, pp 180-196 (2007)

[16] E. FRIDMAN, E. SHWAGERAUS, A. GALPERIN, “Efficient Generation of One-Group Cross Sections for Coupled Monte Carlo Depletion Calculations”, *Nucl. Sci. Eng.*, **159**, pp 37-47 (2008)

[17] M. LAURIE, A. MARMIER , G. BERG , J-M. LAPETITE, M. A. FUTTERER, C. TANG, “Results of the HFR-EU1 Fuel Irradiation of INET and AVR Pebbles in the HFR Petten”, *Nucl. Eng. Des.*, **251**, pp 117-123 (2012)

[18] G. MENARD, S. KNOL, “HFR EU-1 Non-Destructive Examination”, ARCHER Project Deliverable D32.11 (2012)

[19] M. LAURIE, O. SEEGER, “HFR-EU 1/3 and HFR-EU1/4 Gamma Spectrometry Preliminary Results”, ARCHER Project Deliverable D32.12 (2014)

[20] S. C. VAN DER MARCK, “Calculation of Unperturbed Spectra for EU1 Pebbles”, NRG k5042/12.116089 ID/SvdM/IC, NRG, The Netherlands (2012)